Jour. Ind. Inst. Sc. 61 (A), July 1979, Pp. 127-171


# Dielectric-lined rectangular metal waveguide

R. CHATTERJEE AND G. K. DEB*
Department of Electrical Communication Engineering, Indian Institute of Science, Bangalore 560 012.

Received on May 24, 1979

## Abstract

The propagation characteristics of electromagnetic waves in a dielectric-lined rectangular metal waveguide have been studied. The lining on the two side walls (E-plane) together with the air space in between them is considered as a homogeneous equivalent dielectric medium whose equivalent dielectric constant is derived by using electrostatic theory. The theoretical work is based on the fact that LSE and LSM modes can be propagated in a rectangular metal waveguide lined in the two longer sides (H-plane) by dielectric lining. The phase constant, guide wavelength, phase velocity, cut-off frequency, relative intensities, power flow, attenuation constant and power handling capacity of different $LSE_{mn}$ and $LSM_{mn}$ modes have been determined. Experimental verification of the guide wavelength at 'X', 'ku' and 'Ka' bands and cut-off frequency are reported.

Key words: Inhomogeneous waveguide, LSE and LSM modes

## 1. Introduction

The successful development of microwave techniques and their utilization for microwave communication created interest in the design and development of various types of microwave components based on the properties of inhomogeneous waveguides, *viz.*, guides partially loaded with dielectrics, ferrites, etc. Introduction of dielectrics or ferrites in waveguides results in changes of (i) cut-off frequency, (ii) phase constant, (iii) power flow, (iv) band width, (v) phase velocity, (vi) attenuation constant, etc., and may in some cases permit the use of a guide of smaller cross-section for a given cut-off frequency.

Previously several workers have studied rectangular waveguides loaded by dielectric slabs in the *H*-plane[1-8] and rectangular waveguides loaded by dielectric slabs in the *E*-plane[9-22]. The square waveguide with a dielectric lining has been studied by Tsandoulas[23]. In most of these cases, *E* or *H* modes and in some cases LSE, LSM and EH modes have been considered.

* Electronics and Radar Development Establishment, Bangalore 560 001.

In this paper an attempt has been made to make an exhaustive analytical study of as many aspects as possible of the problem of propagation of electromagnetic waves in a dielectric-lined rectangular metal waveguide and verify experimentally some of the theoretical results. The theoretical work has been based on the fact that LSE and LSM modes can be propagated in a rectangular metal waveguide lined on two sides by dielectric lining.[4,5,7]. The lining on the two side walls ($E$-plane) together with the airspace in between them is considered as a homogeneous equivalent dielectric medium whose equivalent dielectric constant has been derived by using electrostatic theory. The work has been motivated by the fact that there is sufficient scope for theoretical and experimental work on the propagation characteristics of a dielectric-lined rectangular metal waveguide on which very little information is available in published literature, and it is felt that this will add to our knowledge of the subject.

Deriving the field components for LSE and LSM modes using Hertz potentials, and applying boundary conditions, the characteristic equations have been derived and solved numerically for varying parameters like dielectric constant and thickness of dielectric coating. The modal analysis shows that the propagating modes can be classified into two categories, namely, (i) completely sinusoidal and (ii) partly sinusoidal and partly hyperbolic. Relative intensities of different $\mathrm{LSE}_{mn}$ and $\mathrm{LSM}_{mn}$ modes, the power flow, attenuation constant, cut-off frequency, phase velocity, group-velocity and power handling capacity (by two methods) have been determined. Experimental verification of the guide wavelength at $X$, ' Ku ' and ' Ka ' bands and of the cut-off frequency are reported.

## 2. Geometry of the problem

The dielectric-lined waveguide (Fig. 1) is divided into five regions and the structure is modified (Fig. 2) by using the concept of equivalent dielectric constant as explained later. It is assumed that the walls of the metal waveguide have infinite conductivity. the dielectric lining has constants $\epsilon_{r_2}, \mu_r = 1, \sigma = 0$, and the equivalent dielectric region 1 of Fig. 1.$b$ has constants $\epsilon_{req}$, $\mu_r = 1$ and $\sigma = 0$.

Considering the three regions 1, 4 and 5 of Fig. 1 as equivalent to three capacitors in series, the equivalent dielectric constant $\epsilon_{req}$ of the composite medium made up of the above three media is derived as follows:

$$\frac{1}{\dfrac{A_1 \epsilon_0 \epsilon_{req}}{a}} = \frac{1}{\dfrac{A_1 \epsilon_0 \epsilon_{r_2}}{d}} + \frac{1}{\dfrac{A_1 \epsilon_0 \epsilon_{r_1}}{(a-2d)}} + \frac{1}{\dfrac{A_1 \epsilon_0 \epsilon_{r_2}}{d}} \tag{1}$$

where $A_1$ = area of the capacitor plate

$\epsilon_0$ = permittivity of free space

and $d$ = thickness of the dielectric lining

Solving eqn. (1) for $\epsilon_{req}$, we obtain

$$\epsilon_{req} = \frac{a \epsilon_{r_1} \epsilon_{r_2}}{2d\, \epsilon_{r_1} + \epsilon_{r_2}(a - 2d)} \tag{2}$$

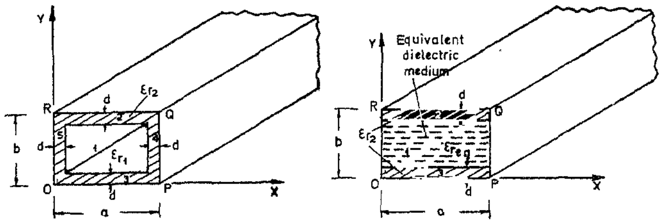


FIG. 1a. Dielectric-lined rectangular waveguide. FIG. 1b. Equivalent of Fig. 1a.

*d*—Dielectric lining thickness; *a*—Width of the guide; *b*—Height of the guide; $\epsilon_{req}$—Equivalent dielectric constant.

FIG. 1. Geometry of the problem.

## 3. Field components

It is known that a rectangular metal waveguide loaded with dielectric lining on the top and bottom *H*-plane faces (Fig. 2), supports LSE and LSM modes[7,14]. Each of these modes are characterized by five field components with $E_y = 0$ and $H_y = 0$ in the case of LSE and LSM modes respectively. The field components of the LSE mode are derived in terms of a magnetic type Hertzian vector potential $\vec{\pi}_M$ and the field components of the LSM mode are derived in terms of an electric type Hertzian vector potential $\vec{\pi}_E$.

## 4. LSE$_{mn}$ mode

The magnetic-type Hertzian vector potential $\vec{\pi}_M$ can be expressed as

$$\vec{\pi}_M = \vec{a}_y \psi_M \tag{3}$$

where the magnetic scalar potential is given by

$$\psi_M = f(x)\, g(y) \exp(j\omega t - \gamma_{mn} z). \tag{4}$$

The electric and magnetic field vectors $\vec{E}$ and $\vec{H}$ are given by

$$\vec{E} = -j\omega\mu_0 \mu_r \nabla X \vec{\pi}_M \tag{5}$$

$$H = \nabla X \frac{\vec{E}}{-j\omega\mu_0 \mu_r} \tag{6}$$

where $\mu_0$ = permittivity of free space = $4\pi \times 10^{-7}$ henry/meter. The field components derived from eqns. (5) and (6) are given by

$$E_{xi} = -j\omega\mu_0\mu_r \; \gamma_{mn} \, \psi_M \tag{7}$$

$$E_{yi} = 0 \tag{8}$$

$$E_{zi} = -j\omega\mu_0 \, \mu_r \frac{\partial \psi_M}{\partial x} \tag{9}$$

$$H_{xi} = \frac{\partial^2 \psi_M}{\partial x \, \partial y} \tag{10}$$

$$H_{yi} = -\left(\gamma_{mn}^2 \psi_M + \frac{\partial^2 \psi_M}{\partial x^2}\right) \tag{11}$$

$$H_{zi} = -\gamma_{mn} \frac{\partial \psi_M}{\partial y} \tag{12}$$

Where $\psi_M$ satisfies the scalar Helmholtz equation

$$\frac{\partial^2 \psi_M}{\partial x^2} + \frac{\partial^2 \psi_M}{\partial y^2} + (\gamma_{mn}^2 + k_0^2 \mu_r \, \epsilon_{r_i}) \psi_M = 0 \tag{13}$$

where

$k_0 = \omega \sqrt{\epsilon_0 \mu_0}$

$i$ = 1,2,3 indicating the regions 1,2,3 (Fig. 2)

$\epsilon_{r_1} = \epsilon_{req}$

$\epsilon_{r_2} = \epsilon_{r_3}$

The solution of eqn. (13) is of the form

$$\psi_M = \begin{Bmatrix} \sin \\ \cos \end{Bmatrix} (k_{yi} \, y) \begin{Bmatrix} \sin \\ \cos \end{Bmatrix} (k_x \, x) \; \exp \, (j\omega t - \gamma_{mn} z) \tag{14}$$

where $k_{yi}$ and $k_x$ denote the transverse propagation constants in the $y$ and $x$ directions respectively. The values of $k_x$ are discrete and equal to $m\pi/a$, where $m$ = 0,1,2, which are determined by applying the proper boundary conditions that $E_z = 0$ at $x = 0$ and at $x = a$.

Assuming that the guide is lossless the longitudinal propagation constant can be written as

$$\gamma_{mn} = j\beta_{mn} \tag{15}$$

where $\beta_{mn}$ should be real for propagation to exist.

Equation (14) can be written in the form

$$\psi_M = g\,(y) \cos \frac{m\pi}{a} x \; \exp \, (j\omega t - \beta_{mn} z). \tag{16}$$

The field components in regions 1,2,3 of Fig. 1 **b**, derived with the aid of eqns. (7) to (12), are as follows:

$$E_{x_i} = \omega\mu_0\mu_r \beta_{mn} [C_i \sin k_{y_i} y + D_i \cos k_{y_i} y]$$

$$\cos \frac{m\pi}{a} x \exp (-j\beta_{mn} z) \tag{17}$$

$$E_{y_i} = 0 \tag{18}$$

$$E_{z_i} = j\omega\mu_0\mu_r \frac{m\pi}{a} [C_i \sin k_{y_i} y + D_i \cos k_{y_i} y]$$

$$\sin \frac{m\pi}{a} x \exp (-j\beta_{mn} z) \tag{19}$$

$$H_{x_i} = -\frac{m\pi}{a} k_{y_i} [C_i \cos k_{y_i} y - D_i \sin k_{y_i} y]$$

$$\times \sin \frac{m\pi}{a} x \exp (-j\beta_{mn} z) \tag{20}$$

$$H_{y_i} = \left(\beta_{mn}^2 + \frac{m^2\pi^2}{a^2}\right) [C_i \sin k_{y_i} y + D_i \cos k_{y_i} y]$$

$$\times \cos \frac{m\pi}{a} x \exp (-j\beta_{mn} z) \tag{21}$$

$$H_{z_i} = -j\beta_{mn} k_{y_i} [C_i \cos k_{y_i} y - D_i \sin k_{y_i} y]$$

$$\cos \frac{m\pi}{a} \times \exp (-j\beta_{mn} z) \tag{22}$$

where $i = 1,2,3$ respectively in the three regions 1,2,3 and $k_{y3} = k_{y2}$. The harmonic time dependence $e^{j\omega t}$ has been omitted for the sake of convenience.

The boundary conditions at the interface of the different regions are:

Between regions 1 and 2, *i.e.*, at $y = (b - d)$,

$$E_{x_1} = E_{x_2},\ H_{x_1} = H_{x_2},\ E_{z_1} = E_{z_2},\ H_{z_1} = H_{z_2} \tag{23}$$

Between regions 1 and 3, *i.e.*, at $y = d$,

$$E_{x_1} = E_{x_3},\ H_{x_1} = H_{x_3},\ E_{z_1} = E_{z_3}$$

and $H_{z_1} = H_{z_3}$. (24)

At $y = b$, $E_{x_2} = E_{z_2} = 0$ (25)

At $y = 0$, $E_{x_3} = E_{z_3} = 0$. (26)

The conditions (25) and (26) give

$$D_2 = -C_2 \tan (k_{y_2} b) \tag{27}$$

and $D_3 = 0.$ (28)

Applying the boundary conditions (23) and (24) and using eqns. (27) and (28), we obtain

$$C_1 \sin (k_{y_1} y) + D_1 \cos (k_{y_1} y_1) - C_3 \sin (k_{y_2} y_1) = 0 \tag{29}$$

$$C_1 k_{y_1} \cos k_{y_1} y_1 - D_1 k_{y_1} \sin (k_{y_1} y_1) - C_3 k_{y_2} \cos (k_{y_2} y_1) = 0 \tag{30}$$

$$\cos (k_{y_2} b) [C_1 \sin (k_{y_1} y_2) + D_1 \cos (k_{y_1} y_2)] + C_2 \sin (k_{y_2} y_1) = 0 \tag{31}$$

$$\cos (k_{y_2} b) [C_1 k_{y_1} \cos (k_{y_1} y_2) - D_1 k_{y_1} \sin (k_{y_1} y_2)] - C_2 k_{y_2} \cos (k_{y_2} y_1) = 0 \tag{32}$$

where $y_1 = d$, $y_2 = b - d$.

For a non-trivial solution of eqns. (29) to (32), the following characteristic equation is satisfied:

$$\begin{vmatrix} \sin (k_{y_1} y_1), \cos (k_{y_1} y_1), \quad 0, \quad - \sin (k_{y_2} y_1) \\ k_{y_1} \cos (k_{y_1} y_1), \ - k_{y_1} \sin (k_{y_1} y_1), \quad 0, \quad - k_{y_2} \cos (k_{y_2} y_1) \\ \cos (k_{y_2} b) \sin (k_{y_1} y_2), \cos (k_{y_2} b), \sin (k_{y_2} y_1), \quad 0, \cos (k_{y_1} y_2) \\ k_{y_1} \cos (k_{y_2} b), \ - k_{y_2} \cos (k_{y_2} b), \ - k_{y_2} \cos (k_{y_2} y_2), 0, \\ \cos (k_{y_1} y_2) \times \sin (k_{y_1} y_2) \end{vmatrix} = 0 \tag{33}$$

which on simplification becomes

$$\begin{aligned} & k_{y_2}^2 \cos^2 (k_{y_2} d) \sin k_{y_1} (b - 2d) \\ & \quad + 2k_{y_1} k_{y_2} \cos (k_{y_2} d) \sin (k_{y_2} d) \cdot \cos k_{y_1} (b - 2d) \\ & \quad - k_{y_1}^2 \sin^2 (k_{y_2} d) \sin k_{y_1} (b - 2d) = 0 \end{aligned} \tag{34}$$

where

$$k_{y_1}^2 = \omega^2 \mu_0 \mu_r \epsilon_0 \epsilon_{req} - \beta_{mn}^2 - \frac{m^2 \pi^2}{a^2} \tag{35}$$

and

$$k_{y_2}^2 = \omega^2 \mu_0 \mu_r \epsilon_0 \epsilon_{r_2} - \beta_{mn}^2 - \frac{m^2 \pi^2}{a^2} \tag{36}$$

### 5. $LSM_{mn}$ mode

The field components are derived in this case with the aid of the electric-type Hertzian vector potential $\vec{\pi}_e$ given by

$$\vec{\pi}_e = \mathbf{a}_y \psi_E \tag{37}$$

where the electric scalar potential $\psi_E$ is given by

$$\psi_E = h(x)\, l(y)\, \exp\,(j\omega t - \gamma_{mn} z). \tag{38}$$

The magnetic and electric field vectors **H** and **E** are expressed as

$$\mathbf{H} = j\omega\epsilon_0\, \epsilon_{r_i} \nabla \times \vec{\pi}_E \tag{39}$$

$$\mathbf{E} = \nabla \times \left(\frac{\mathbf{H}}{j\omega\epsilon_0\, \epsilon_{r_i}}\right) \tag{40}$$

where $i = 1,2,3$ refer to the regions 1,2,3 in Fig. 2. The field components derived from eqns. (39) and (40) are given by

$$H_{z_i} = j\omega\epsilon_0\, \epsilon_{r_i}\, \gamma_{mn} \psi_E \tag{41}$$

$$H_{y_i} = 0 \tag{42}$$

$$H_{x_i} = j\omega\epsilon_0\, \epsilon_{r_i} \frac{\delta\psi_E}{\delta x} \tag{43}$$

$$E_{x_i} = \frac{d^2\, \psi_E}{dx\, \delta y} \tag{44}$$

$$E_{y_i} = -\left(\gamma_{mn}^2 \psi_E + \frac{d^2\, \psi_E}{dx^2}\right) \tag{45}$$

$$E_{z_i} = -\, \gamma_{mn} \frac{d\psi_E}{dy} \tag{46}$$

Proceeding in a similar way as in the case of the $LSE_{mn}$ mode, the solution of the scalar Helmholtz eqn. (13) is of the form

$$\psi_E = l\,(y)\, \sin \frac{m\pi}{a} x \exp\,(j\omega t - \gamma_{mn} z)$$

$$= (G_i \sin\, k_{y_i} y + H_i \cos\, k_{y_i} y)\, \sin \frac{m\pi}{a} x \exp\,(j\omega t - \gamma_{mn} z) \tag{47}$$

where $i = 1,2,3$ in the three regions 1,2,3.

Using eqns. (41) to (47), and applying the boundary conditions given by eqns. (23) to (26), we obtain the characteristic equation for $LSM_{mn}$ modes as

$$\begin{aligned} &\epsilon_{r_2}^2 k_{y_1}^2 \cos^2\, (ky_2\, d)\, \sin\, k_{y_1}(b - 2d) \\ &+ 2\epsilon_{req}\, \epsilon_{r_2} k_{y_1} k_{y_2} \cos\, (k_{y_2} d)\, \sin\, (k_{y_2} d) \cos\, k_{y_1}(b - 2d) \\ &- \epsilon_{req}^2\, k_{y_2}^2 \sin^2 (k_{y_2} d)\, \sin\, k_{y_1}\, (b - 2d) = 0 \end{aligned} \tag{48}$$

where $k_{y_1}^2$ and $k_{y_2}^2$ are given by eqns. (35) and (36),

## 6. Solution of the characteristic equations for LSE and LSM modes

It is found that the solution of the characteristic eqns. (34) and (48) for $LSE_{mn}$ and $LSM_{mn}$ modes respectively, exist only when the transverse propagation constant $k_{y_2}$ is real. But $k_{y_1}$ may be real or imaginary, which means that

$$\omega^2 \mu_0 \mu_r \epsilon_0 \epsilon_{r_2} > \left(\beta_{mn}^2 + \frac{m^2 \pi^2}{a^2}\right) \tag{49}$$

In order that $k_{y_2}$ is real, but $k_{y_1}$ is real or imaginary, the following inequality condition must be satisfied,

$$\omega^2 \mu_0 \mu_r \epsilon_0 \epsilon_{req} \gtrless \left(\beta_{mn}^2 + \frac{m^2 \pi^2}{a^2}\right), \tag{50}$$

which means that $| k_{y_2} |^2$ is always greater than $| k_{y_1} |^2$. This is justified as the computation of $\epsilon_{req}$ shows that $\epsilon_{r_2}$ is always greater than $\epsilon_{req}$.

It is also observed that when $k_{y_2}$ is always real and $k_{y_1}$ is real, the characteristic equation is expressed only in terms of circular trigonometric sine and cosine functions. However, when $k_{y_1}$ is imaginary and $k_{y_2}$ is real, the characteristic equation will involve not only circular trigonometric functions but also hyperbolic functions. We may designate these solutions of eqns. (34) and (48) as (1) a completely sinusoidal mode ($k_{y_1}$ and $k_{y_2}$ are both real and positive) designated as Mode 1 and (2) partly sinusoidal and partly hyperbolic mode ($k_{y_1}$ is imaginary and $k_{y_2}$ is real and positive) designated as Mode 2.

If, however, $k_{y_2}$ is imaginary, or in other words,

$$\omega^2 \mu_0 \mu_r \epsilon_0 \epsilon_{r_2} < \left(\beta_{mn}^2 + \frac{m^2 \pi^2}{a^2}\right) \tag{51}$$

the characteristic equation will involve only hyperbolic functions and the modes obtained from the solution may then be identified as completely hyperbolic mode. But when the characteristic equation involves only hyperbolic functions it is found that there is no solution. Hence it is concluded that the completely hyperbolic modes cannot exist. The non-existence of the completely hyperbolic modes can be justified by the following argument. The characteristic equation for this mode, if it exists, is given by:

$$\begin{aligned} & k_{y_2r}^2 \cosh^2 (k_{y_2r} d) \sinh (k_{y_1r} (b-2)) \\ & + 2k_{y_1r} k_{y_2r} \cosh (k_{y_2r} d) \sinh (k_{y_2r} d) \cosh (k_{y_1r} (b-2d)) \\ & + k_{y_1r}^2 \sinh^2 (k_{y_2r} d) \sinh (k_{y_1r} (b-2d)) = 0 \end{aligned} \tag{52}$$

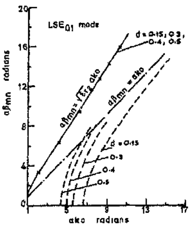


Fig. 2.1–Normalized phase constant $a\beta_{mn}$ vs $ako$ for $LSE_{01}$ mode

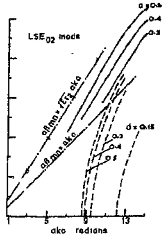


Fig. 2.2–Normalized phase constant $a\beta_{mn}$ vs. $ako$ for $LSE_{02}$ mode

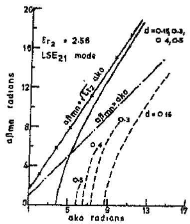


Fig. 2.5–Normalized phase constant $a\beta_{mn}$ vs. $ako$ for $LSE_{21}$ mode

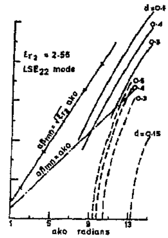


Fig. 2.6–Normalized phase constant $a\beta_{mn}$ vs. $ako$ for $LSE_{22}$ mode

— — — Mode 1, ——— Mode 2, $\varepsilon_{r2}$ = 2.56

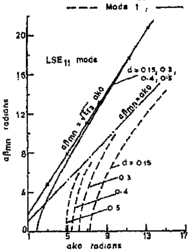


Fig. 2.3–Normalized phase constant $a\beta_{mn}$ vs $ako$ for $LSE_{11}$ mode

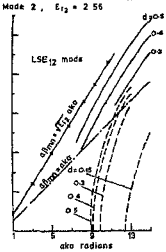


Fig. 2.4–Normalized phase constant $a\beta_{mn}$ vs. $ako$ for $LSE_{12}$ mode

— — — Mode 1, ——— Mode 2

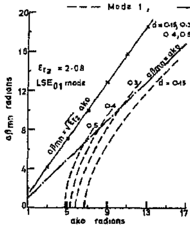


Fig. 2.7–Normalized phase constant $a\beta_{mn}$ vs $ako$ for $LSE_{01}$ mode

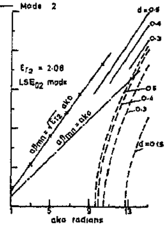


Fig. 2.8–Normalized phase constant $a\beta_{mn}$ vs. $ako$ for $LSE_{02}$ mode

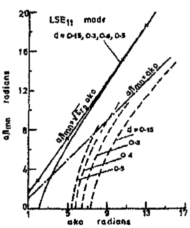


Fig. 2.9–Normalized phase constant $a\beta_{mn}$ vs. $ako$ for $LSE_{11}$ mode

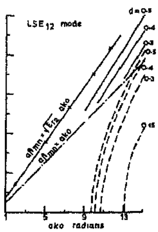


Fig. 2.10–Normalized phase constant $a\beta_{mn}$ vs $ako$ for $LSE_{12}$ mode

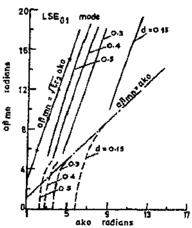


Fig. 2.13–Normalized phase constant $a\beta_{mn}$ vs $ako$ for $LSE_{01}$ mode

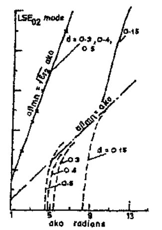


Fig. 2.14–Normalized phase constant $a\beta_{mn}$ vs $ako$ for $LSE_{02}$ mode

— — — Mode 1, ——— Mode 2, $\varepsilon_{r2}$ = 2.08

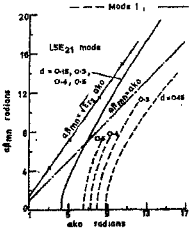


Fig. 2.11–Normalized phase constant $a\beta_{mn}$ vs. $ako$ for $LSE_{21}$ mode

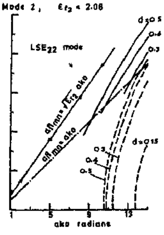


Fig. 2.12–Normalized phase constant $a\beta_{mn}$ vs. $ako$ for $LSE_{22}$ mode

— — — Mode 1, ——— Mode 2, $\varepsilon_{r2}$ = 9.0

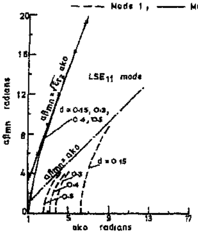


Fig. 2.15–Normalized phase constant $a\beta_{mn}$ vs $ako$ for $LSE_{11}$ mode

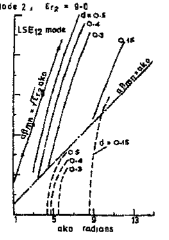


Fig. 2.16–Normalized phase constant $a\beta_{mn}$ vs $ako$ for $LSE_{12}$ mode

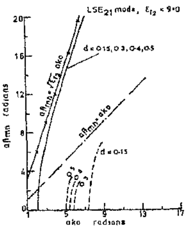


Fig 2.17-Normalized phase constant $\alpha\beta_{mn}$ vs ako for LSE$_{21}$ mode

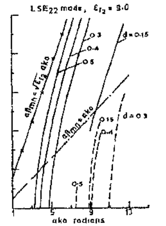


Fig 2.18-Normalized phase constant $\alpha\beta_{mn}$ vs ako for LSE$_{22}$ mode

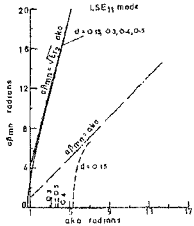


Fig 2.21-Normalized phase constant $\alpha\beta_{mn}$ vs ako for LSE$_{11}$ mode

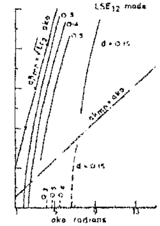


Fig 2.22-Normalized phase constant $\alpha\beta_{mn}$ vs ako for LSE$_{12}$ mode

— — — Mode 1, ——— Mode 2

— · — Mode 1, ——— Mode 2, $\epsilon_{r2}$ = 16·0

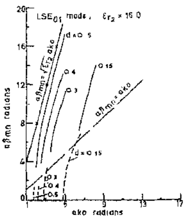


Fig. 2.19-Normalized phase constant $\alpha\beta_{mn}$ vs. ako for LSE$_{01}$ mode

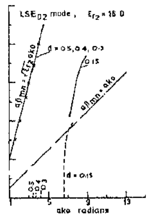


Fig. 2.20-Normalized phase constant $\alpha\beta_{mn}$ vs ako for LSE$_{02}$ mode

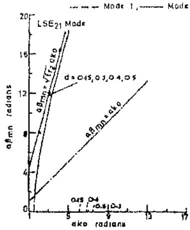


Fig 2.23-Normalized phase constant $\alpha\beta_{mn}$ vs ako for LSE$_{21}$ mode

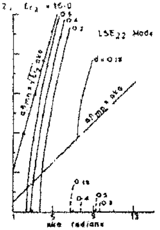


Fig 2.24-Normalized phase constant $\alpha\beta_{mn}$ vs ako for LSE$_{22}$ mode

FIG. 2 -NORMALIZED PHASE CONSTANT $\alpha\beta_{mn}$ Vs ako FOR LSE$_{mn}$ MODE (Parameter being d)

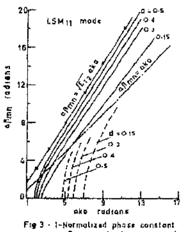


Fig 3-1-Normalized phase constant $\alpha\beta_{mn}$ vs. ako for LSM$_{11}$ mode

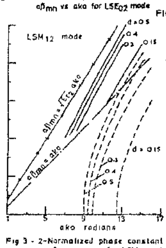


Fig 3-2-Normalized phase constant $\alpha\beta_{mn}$ vs ako for LSM$_{12}$ mode

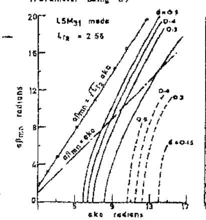


Fig 3-5-Normalized phase content $\alpha\beta_{mn}$ vs ako for LSM$_{31}$ mode

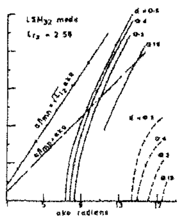


Fig 3-6-Normalized phase constant $\alpha\beta_{mn}$ vs ako for LSM$_{32}$ mode

— — — Mode 1, ——— Mode 2, $\epsilon_{r2}$ = 2·56

— — — Mode 1, ——— Mode 2,

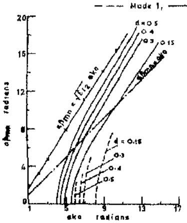


Fig.3-3-Normalized phase constant $\alpha\beta_{mn}$ vs. ako for LSM$_{21}$ mode

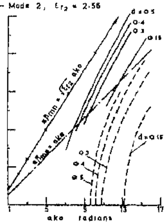


Fig.3-4-Normalized phase constant $\alpha\beta_{mn}$ vs. ako for LSM$_{22}$ mode

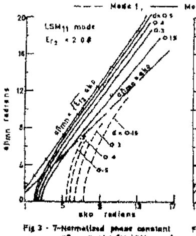


Fig 3-7-Normalized phase constant $\alpha\beta_{mn}$ vs. ako for LSM$_{11}$ mode

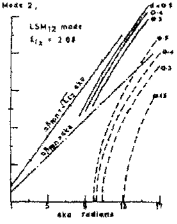


Fig 3-8-Normalized phase constant $\alpha\beta_{mn}$ vs. ako for LSM$_{12}$ mode

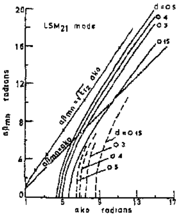


Fig 3 - 9-Normalized phase constant $a\beta_{mn}$ vs ako for LSM$_{21}$ mode

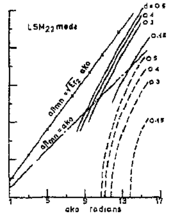


Fig 3 - 10-Normalized phase constant $a\beta_{mn}$ vs ako for LSM$_{22}$ mode

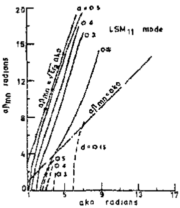


Fig 3 13-Normalized phase constant $a\beta_{mn}$ vs ako for LSM$_{11}$ mode

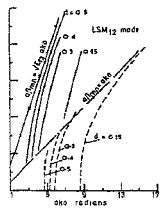


Fig 3 - 14-Normalized phase constant $a\beta_{mn}$ vs. ako for LSM$_{12}$ mode

— — — Mode 1, ——— Mode 2, $\epsilon_{r2}$ = 2.08

— — — Mode 1, ——— Mode 2, $\epsilon_{r2}$ = 9.0

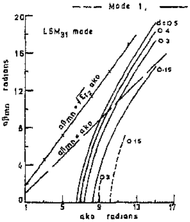


Fig 3 - 11-Normalized phase constant $a\beta_{mn}$ vs. ako fro LSM$_{31}$ mode

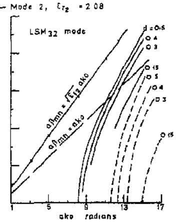


Fig 3 12-Normalized phase constant $a\beta_{mn}$ vs ako for LSM$_{32}$ mode

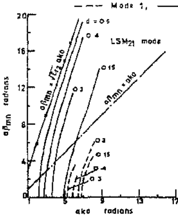


Fig.3 - 15-Normalized phase constant $a\beta_{mn}$ vs ako for LSM$_{21}$ mode

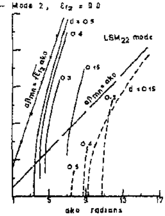


Fig 3 - 16-Normalized phase constant $a\beta_{mn}$ vs ako for LSM$_{22}$ mode

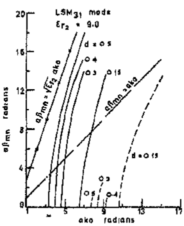


Fig 3 17-Normalized phase constant $a\beta_{mn}$ vs. ako for LSM$_{31}$ mode

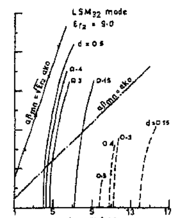


Fig 3 - 18-Normalized phase constant $a\beta_{mn}$ vs. ako for LSM$_{32}$ mode

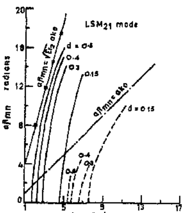


Fig 3 - 21-Normalized phase constant $a\beta_{mn}$ vs ako for LSM$_{21}$ mode

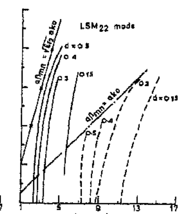


Fig 3 22-Normalized phase constant $a\beta_{mn}$ vs ako for LSM$_{22}$ mod

— — — Mode 1, ——— Mode 2

— — — Mode 1, ——— Mode 2, $\epsilon_{r2}$ = 15.0

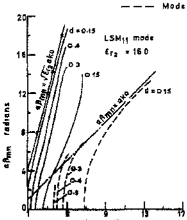


Fig. 3 - 19-Normalized phase constant $a\beta_{mn}$ vs ako for LSM$_{11}$ mode

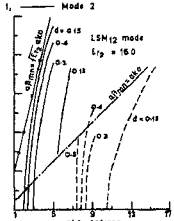


Fig 3 - 20-Normalized phase constant $a\beta_{mn}$ vs ako for LSM$_{12}$mode

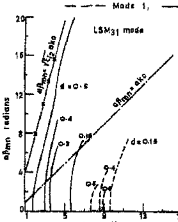


Fig.3 - 23-Normalized phase constant $a\beta_{mn}$ vs. ako for LSM$_{31}$ mode

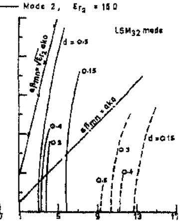


Fig 3 - 24-Normalized phase constant $a\beta_{mn}$ vs. ako for LSM$_{32}$ mode

FIG. 3 -NORMALIZED PHASE CONSTANT $a\beta_{mn}$ Vs ako FOR LSM$_{mn}$ MODE

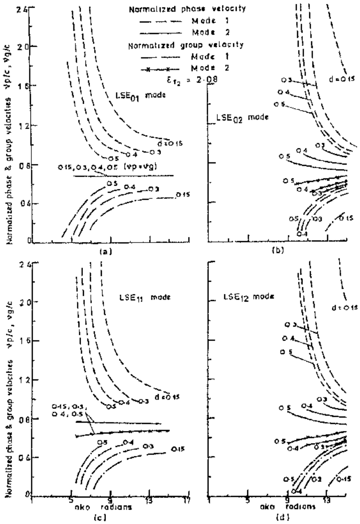


FIG. 4.1—NORMALIZED PHASE AND GROUP VELOCITIES Vs. ako RADIANS (parameter being d)

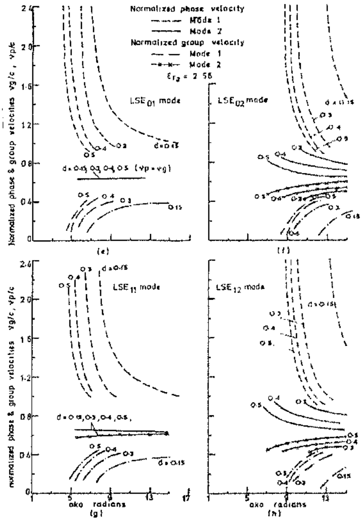


FIG. 4.2—NORMALIZED PHASE AND GROUP VELOCITIES Vs. ako RADIANS

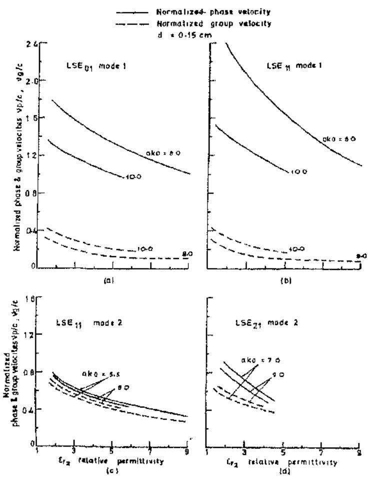


FIG. 4.3—NORMALIZED PHASE AND GROUP VELOCITIES Vs. RELATIVE PERMITTIVITY

## 7. Numerical computations for LSE$_{mn}$ and LSM$_{mn}$ modes

Numerical computations of the different propagation characteristics like the axial phase constant $\beta_{mn}$, the guide wavelength $\lambda_{g_{mn}} = 2\pi/\beta_{mn}$, the phase velocity $v_{p_{mn}} = \omega/\beta_{mn}$, the group velocity

$$v_{g_{mn}} = \frac{d\omega}{d\beta_{mn}} = \frac{c}{\sqrt{\epsilon_{r_2}}}\left[1 - \frac{k_{y_2}^2 + \frac{m^2\pi^2}{a^2}}{\omega^2 \epsilon_0 \mu_0 \epsilon_{r_2}}\right]^{\frac{1}{2}}$$

the cut-off frequency $f_{c_{mn}}$, and attenuation constant below cut-off for dominant and higher order modes have been made. Figs. 2.1 to 3.6 present the normalized phase constant a $\beta_{mn}$ *vs.* $ak_0$ for different LSE and LSM modes respectively for various values of $d$ and $\epsilon_{r_2}$. Figs. 4.1 to 5.2 present the normalized phase and group velocities for various LSE and LSM modes respectively *vs.* $ak_0$ for various values of $d$ and $\epsilon_{r_2}$.

where $k_{y_1} = jk_{y_1}$, and $k_{y_2} = jk_{y_{2r}}$ and $k_{y_{1r}}$ and $k_{y_{2r}}$ are real and positive. Equation (52) is satisfied if and only if all the terms of this equation are zero at the same time. This means that $k_{y_{1r}}$ and $k_{y_{2r}}$ simultaneously become zero. Since $k_{y_{1r}}$ and $k_{y_{2r}}$ satisfy the equations

$$\beta^2_{mn} = \epsilon_{r_2} k_0^2 + k^2_{y_{2r}} - \frac{m^2 \pi^2}{a^2} \tag{53}$$

and

$$\beta^2_{mn} = \epsilon_{req} k_0^2 + k^2_{y_{1r}} - \frac{m^2 \pi^2}{a^2} \tag{54}$$

both $k_{y_{1r}}$ and $k_{y_{2r}}$ cannot become zero. Hence it can be concluded that the characteristic eqn. (52) does not have any solution for the complete hyperbolic modes.

In the case of partly sinusoidal and partly hyperbolic modes the transverse propagation constant in region 1 is

$$k_{y_1} = jk_{y_{1r}} \tag{55}$$

where $k_{y_{1r}}$ is a real positive quantity. In this case the characteristic eqns. (34) and (48) for $LSE_{mn}$ and $LSM_{mn}$ modes respectively become

$$\begin{aligned} & k^2_{y_2} \cos^2 (k_{y_2} d) \sinh (k_{y_{1r}} (b - 2d)) \\ & + 2k_{y_2} k_{y_{1r}} \cos (k_{y_2} d) \sin (k_{y_2 d}) \cosh k_{y_{1r}} (b - 2d) \\ & + k^2_{y_{1r}} \sin^2 (k_{y_2} d) \cdot \sinh \cdot k_{y_{1r}} (b - 2d) = 0 \end{aligned} \tag{56}$$

and

$$\begin{aligned} & - \epsilon^2_{r_2} k^2_{y_{1r}} \cos^2 (k_{y_2} d) \sinh k_{y_{1r}} (b - 2d) \\ & + 2 \epsilon_{req} \epsilon_{r_2} k_{y_{1r}} k_{y_2} \cos (k_{y_2} d) \sinh (k_{y_2} d) \,.\, \cosh (k_{y_{1r}} (b - 2d)) \\ & - \epsilon^2_{req} k^2_{y_2} \sin^2 (k_{y_2} d) \\ & - \epsilon^2_{req} k^2_{y_2} \sin^2 (k_{y_2} d) \sinh (k_{y_{1r}} (b - 2d)) = 0 \end{aligned} \tag{57}$$

where

$$k^2_{y_{1r}} = \beta^2_{mn} + \frac{m^2 \pi^2}{a^2} - \epsilon_{req} k_0^2 \tag{58}$$

and $k_{y_2}$ is given by eqn. (36).

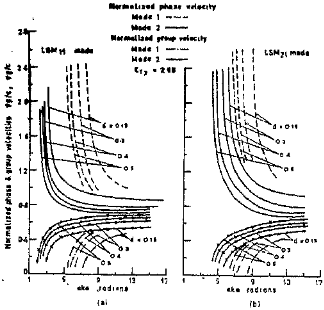

FIG. 5.1. Normalized phase and group velocities vs. $ak_o$ for $LSM_{mn}$ mode (Parameter being d).

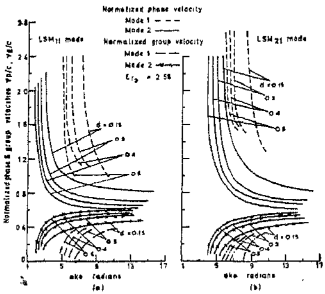

FIG. 5.2. Normalized phase and group velocities vs. $ak_o$ for $LSM_{mn}$ mode.

## 8. Cut-off frequency of $LSE_{mn}$ and $LSM_{mn}$ modes

The cut-off condition is determined by putting $\beta_{mn} = 0$ in eqns. (35) and (36). For modes type 1, both $k_{y_1}$ and $k_{y_2}$ are real and therefore eqn. (35) becomes

$$k_{y_1}^2 = \omega^2 \mu_0 \mu_r \epsilon_0 \epsilon_{req} - \beta_{mn}^2 - \frac{m^2 \pi^2}{a^2} \geq 0$$

and hence at cut-off,

$$k_{y_{1c}}^2 = \epsilon_{req} k_{0c_1}^2 - \frac{m^2 \pi^2}{a^2} \geq 0 \qquad (59)$$

where the subscript $c$ indicates the values at cut-off, and

$$k_{0c_1}^2 = \omega_{c1}^2 \mu_0 \epsilon_0.$$

Hence for mode 1, the cut-off condition is given by

$$\omega_{c1}^2 \geq \frac{1}{\epsilon_{req}} \frac{m^2 \pi^2}{a^2} c^2 \qquad (60)$$

or

$$f_{c_1} \geq \frac{mc}{2a\sqrt{\epsilon_{req}}} \qquad (61)$$

Similarly for mode 2 to exist, $k_{y_2}$ is real and $k_{y_1}$ is imaginary, and the cut-off condition for the mode is derived from eqn. (35) as

$$k_{y_c}^2 = \epsilon_{req} k_{0c2}^2 - \frac{m^2 \pi^2}{a^2} \leq 0 \qquad (62)$$

where $k_{0c_2}^2 = \omega_{c_2}^2 \mu_0 \epsilon_0$

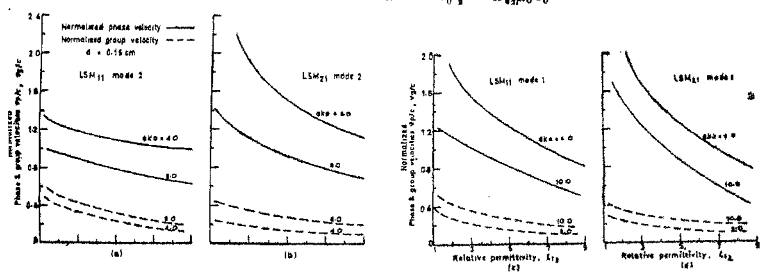

FIG. 5.3. Normalized phase and group velocities vs. $\epsilon_{r_2}$ for $LSM_{mn}$.

which yields

$$\omega_{c_2}^2 \leq \frac{1}{\epsilon_{req}} \frac{m^2 \pi^2}{a^2} c^2 \tag{63}$$

or

$$f_{c_2} \leq \frac{mc}{2a\sqrt{\epsilon_{req}}} \tag{64}$$

It is evident that the cut-off frequency for mode 2 is lower than that of mode 1. Equations (59) and (62) are solved for obtaining the cut-off frequencies for both $LSE_{mn}$ and $LSM_{mn}$ modes.

Figures 6.1 to 7 present the normalized cut-off frequency $ak_{0c}$ *vs.* filling factor $d/a$ for $LSE_{mn}$ and $LSM_{mn}$ modes respectively. Figs. 8.1 to 9 present the normalized cut-off frequency $ak_{0c}$ *vs.* relative permittivity $\epsilon_{r_2}$ for $LSE_{mn}$ and $LSM_{mn}$ modes respectively.

## 9. Bandwidth

The percentage bandwidth is defined as

$$B_w = 200 \times \frac{f_c^+ - f_c^-}{f_c^+ + f_c^-} \tag{65}$$

where $f_c^-$ = cut-off frequency of the lowest mode

$f_c^+$ = cut-off frequency of the next higher order mode.

The percentage bandwidth of the $LSE_{mn}$ and $LSM_{mn}$ modes has been calculated as a function of dielectric filling factor $d/a$ and $\epsilon_{r_2}$, and the results are shown in Figs. 10 and 11.

## 10. Attenuation constant below cut-off

In the region below cut-off the square of the transverse propagation constants $k_{y_1}^2$ and $k_{y_2}^2$ are real, and the modes below cut-off are non-propagating. $\gamma_{mn}^2$ can be written as

$$\gamma_{mn}^2 = a_{mn}^2 \tag{66}$$

and $a_{mn}$ satisfies the equations

$$k_{y_2}^2 = \epsilon_{r_2} k_0^2 + a_{mn}^2 - \frac{m^2 \pi^2}{a^2} \tag{67}$$

$$k_{y_1}^2 = \epsilon_{req} k_0^2 + a_{mn}^2 - \frac{m^2 \pi^2}{a^2} \tag{68}$$

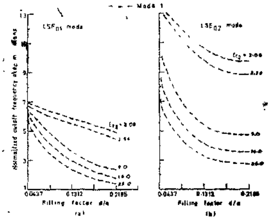

FIG. 6.1. Normalized cut off frequency $ak_{oe}$ vs. filling factor d/a.

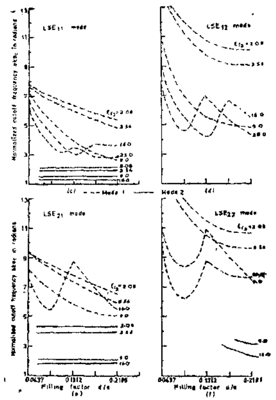

FIG. 6.2. Normalized cut off frequency $ak_{oe}$ vs. filling factor d/a.

The attenuation constant below cut-off $\alpha_{mn}$ has been calculated for both LSE$_{mn}$ modes and LSM$_{mn}$ modes and are shown in Figs. 12 and 13 respectively.

## 11. Relative intensities of the field components of LSE$_{mn}$ and LSM$_{mn}$ modes

For LSE$_{mn}$ modes, (eqns. (29) to (32)), three of the amplitude constants $C_1$, $D_2$, $C_2$, $C_3$ can be expressed in terms of one of them, say $C_2$, and hence their relative amplitudes can be calculated. Equations (27) and (28) give the values of $D_2$ and $D_3$. It is similar for LSM$_{mn}$ modes.

Using the calculated values of the above amplitude constants, the relative intensities of the field components for LSE$_{mn}$ and LSM$_{mn}$ modes are calculated and presented in Figs. 14. 1 to 15. 2 respectively.

## 12. Orthogonal properties of the fields of LSE$_{mn}$ and LSM$_{mn}$ modes

The following orthogonal relation holds good for LSE$_{mn}$ and LSM$_{mn}$ modes[14] in the dielectric-lined rectangular metal waveguide

$$\iint_S \mathbf{E}_{t\,(mn)} \times \mathbf{H}_{t\,(pq)} \cdot \mathbf{a}_z \, da = 0 \tag{69}$$

where $m \neq p$ and $n \neq q$ or both, and $S$ denotes the cross-section of the lined waveguide, $\mathbf{E}_{t\,(mn)}$ is the transverse electric field for the '$mn$'th mode. For a lossy medium, $\mathbf{H}_{t\,(pq)}$ is placed by $\mathbf{H}^*_{t\,(pq)}$ so that

$$\iint_S \mathbf{E}_{t\,(mn)} \times \mathbf{H}^*_{t\,(pq)} \cdot \mathbf{a}_z \, ds = 0. \tag{70}$$

Further in the case of LSE$_{mn}$ modes the transverse electric fields for two different modes are orthogonal. The same is also true for the transverse and the longitudinal magnetic field components which is as follows :

$$\iint_S \mathbf{E}_{t\,(mn)} \cdot \mathbf{E}_{t\,(pq)} \, da = 0$$

$$\iint_S \mathbf{H}_{t\,(mn)} \cdot \mathbf{H}_{t\,(pq)} \, da = 0 \tag{71}$$

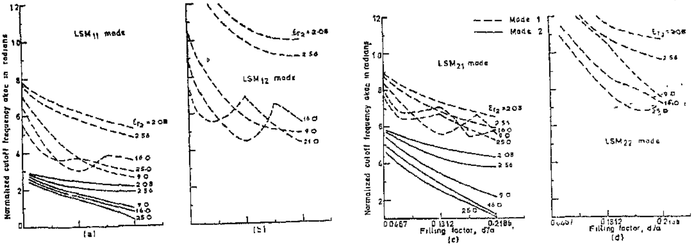


FIG. 7. Normalized cut off frequency $ak_{oc}$ vs. filling factor d/a for $LSM_{mn}$ mode.

$$\iint_S E_{z\,(mn)} \cdot E_{z\,(pq)}\, da = 0$$

$$\iint_S H_{z\,(mn)} \cdot H_{z\,(pq)}\, da = 0.$$

None of the orthogonal properties given by eqn. (71) hold good for $LSM_{mn}$ modes. The orthogonal properties of $LSM_{mn}$ modes can be treated as described by collin[14].

The above orthogonal properties are used to evaluate the total power flow by the summation of the power flow in each region carried by each non-degenerate mode individually.

## 13. Power flow for $LSE_{mn}$ and $LSM_{mn}$ modes

The average power flow along the positive longitudinal $z$-direction is calculated by using the relation

$$P_z = \tfrac{1}{2}\ \mathrm{Re} \iint_S (\mathbf{E}_t \times \mathbf{H}_t) \cdot \mathbf{a}_z\, dy\, dx \tag{72}$$

where $S$ is the cross-section of the lined waveguide. The total power flow is the sum of the power $P_{z_1}$ carried inside the region $(d \leqslant y \leqslant (b-d))$, the power $P_{z_2}$ in the region $2\,((b-d) \leqslant y \leqslant b)$; and the power $P_{z_3}$ in the region $3\,(0 \leqslant y \leqslant d)$ (Fig. 2).

For $LSE_{mn}$ modes, $E_{y_i} = 0$ $(i = 1,2,3)$, and hence the total power flow $P_{zT}$ is given by

$$P_{zT\,(\mathrm{LSE})} = \tfrac{1}{2}\ \mathrm{Re} \int_0^a \Big[ \int_d^{(b-d)} (E_{x_1} H_{y_1}^*\, dy + \int_{(b-d)}^{b} E_{x_2} H_{y_2}^*\ dy + \int_0^d E_{x_3} H_{y_3}^*\, dy\Big]\, dx \tag{73}$$

Substituting the expressions for the appropriate field components from eqns. (17) to (22), we obtain

$$\frac{P_{zT\,(\mathrm{LSE})}}{|\,C_3\,|^2} = \frac{a\omega\mu_0\mu_r\beta_{mn}}{2N_0}\left(\beta_{mn}^2 + \frac{m^2\pi^2}{a^2}\right) \cdot \mathrm{Re}\Big[\,|\,E_1\,|^2 \frac{b-2d}{2} - \frac{\sin 2k_{y_1}(b-2d)}{4k_{y_1}}$$

$$+\,|\,F_1\,|^2 \left(\frac{b-2d}{2} + \frac{\sin 2k_{y_1}(b-2d)}{2k_{y_1}}\right)$$

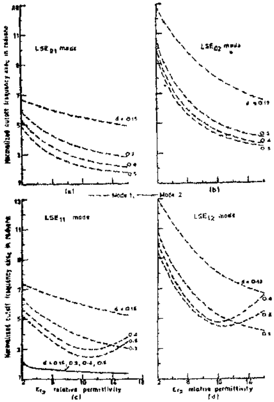


FIG. 8.1. Normalized cut off frequency vs. relative permittivity $\epsilon_{r_2}$.

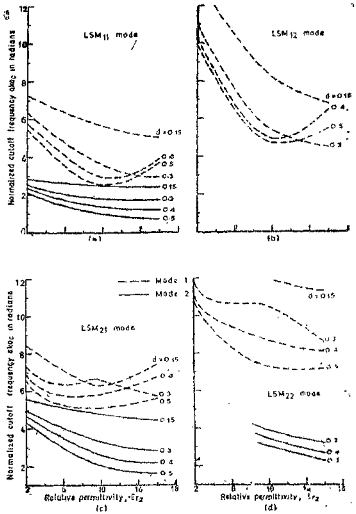


FIG. 9. Normalized cut off frequency $ak_{oc}$ vs. relative permittivity $\epsilon_{r_2}$ for LSM$_{mn}$ mode.

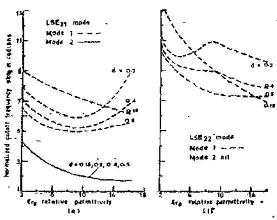


FIG. 8.2. Normalized cut off frequency vs. relative permittivity $\epsilon_{r_2}$.

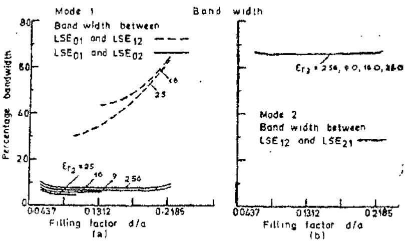


FIG. 10. Percentage bandwidth vs. filling factor d/a for LSE$_{mn}$ mode.

$$+ (E_1F_1^* + E_1^* F_1) \frac{\sin^2 k_{y_1}(b-2d)}{2k_{y_1}} + |E_3|^2 \left(\frac{d}{2} - \frac{\sin 2k_{y_3} d}{4k_{y_3}}\right)$$

$$+ |F_2|^2 \left(\frac{d}{2} + \frac{\sin 2k_{y_2} d}{4k_{y_2}}\right) + (E_2F_2^* + E_2^* F_2) \frac{\sin^2 k_{y_2} d}{2k_{y_2}}$$

$$+ \left(\frac{d}{2} - \frac{\sin 2k_{y_3} d}{4k_{y_3}}\right)\Bigg] \tag{74}$$

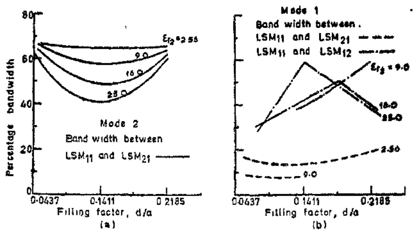


FIG. 11. Percentage bandwidth vs. filling factor d/a for $LSM_{mn}$ mode.

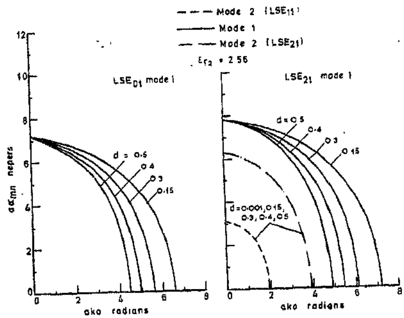


FIG. 12. Normalized attenuation $a\alpha_{mn}$ below cut off vs. $ak_o$ for $LSE_{mn}$ mode.

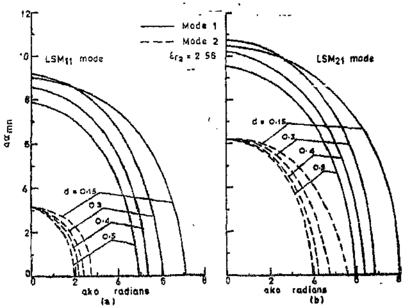


FIG. 13. Normalized attenuation constant $a\alpha_{mn}$ below cut off vs. $ak_o$ for $LSM_{mn}$ mode.

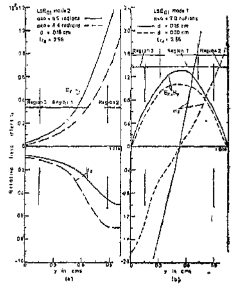

FIG. 14.1. Relative field intensity along $y$-direction for $LSE_{01}$ mode.

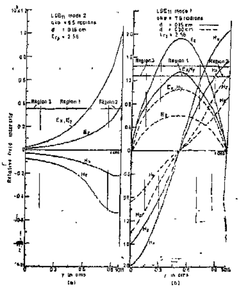

FIG. 14.2. Relative field intensity along $y$-direction for $LSE_{11}$ mode.

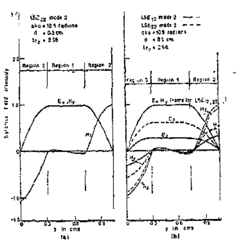

FIG. 14.3. Relative field intensity along $y$-direction for $LSE_{02}$, $LSE_{12}$ and $LSE_{22}$ modes.

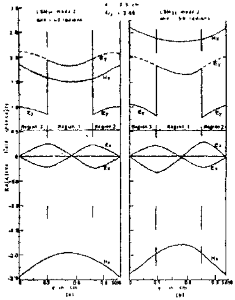

FIG. 15·1. Relative field intensity along $y$-direction for $LSM_{11}$ and $LSM_{21}$ modes 2.

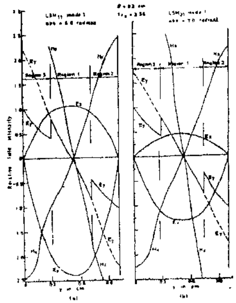

FIG. 15·2. Relative field intensity along $y$-direction for $LSM_{11}$ and $LSM_{21}$ modes 1.

where $N_0$ is the Nuemann factor given by

$$\begin{aligned} N_0 &= 1 \text{ when } m = 0 \\ &= 2 \text{ when } m = 1,2,3 \end{aligned} \tag{75}$$

and

$$\begin{aligned} E_1 &= \frac{k_{y_2}}{k_{y_1}} \cos k_{y_2} d \\ F_1 &= \sin k_{y_2} d \end{aligned} \tag{76}$$

$$\begin{aligned} E_2 &= \cos k_{y_2} \cos k_{y_1} (b - 2d) - \frac{k_{y_1}}{k_{y_2}} \sin k_{y_2} d \sin k_{y_1} (b - 2d) \\ F_2 &= \frac{k_{y_2}}{k_{y_1}} \cos k_{y_2} d \sin k_{y_1} (b - 2d) + \sin k_{y_2} d \cos k_{y_1} (b - 2d) \end{aligned} \tag{77}$$

Similarly for $LSM_{mn}$ modes, the total power flow is given by

$$\frac{P_{zT\,(\mathrm{LSM})}}{|H_3|^2} = \frac{1}{4}\, \omega \epsilon_0\, a\beta_{mn} \left(\beta_{mn}^2 + \frac{m^2 \pi^2}{a^2}\right)$$

$$\times \mathrm{Re}\Big[\, |\epsilon_{\mathrm{req}}| \Big\{ |T_1|^2 \left(\frac{b-2d}{2} - \frac{\sin 2k_{y_1}(b-2d)}{4k_{y_1}}\right)$$

$$+ |S_1|^2 \left(\frac{b-2d}{2} - \frac{\sin 2k_{y_1}(b-2d)}{4k_{y_1}}\right)\Big\}$$

$$+\left\{(T_1S_1^* + T_1^* S_1)\frac{\sin\ 2k_{y_1}(b-2d)}{2k_{y_1}}\right\}$$
$$+\mid \epsilon_{r_2}\mid \left\{\mid T_2\mid^2\left(\frac{d}{2}-\frac{\sin 2k_{y_2} d}{4k_{y_2}}\right)+\mid S_2\mid^2\left(\frac{d}{2}+\frac{\sin 2k_{y_2} d}{4k_{y_2}}\right)\right.$$
$$\left.+(T_2S_2^* + T_2^* S_2)\frac{\sin^2 k_{y_2} d}{2k_{y_2}}\right\}+\mid \epsilon_{r_3}\mid\left(\frac{d}{2}+\frac{\sin 2k_{y_2} d}{4k_{y_2}}\right)\Bigg] \tag{78}$$

where

$H_3$ is an amplitude factor for $LSM_{mn}$ modes corresponding to $C_3$ for $LSE_{mn}$ modes,

$$T_1 = -\frac{k_{y_2}}{k_{y_1}}\ \sin\ k_{y_2} d$$

$$S_1 = \frac{\epsilon_{r2}}{\epsilon_{req}}\ \cos\ k_{y_2} d$$

$$T_2 = -\sin k_{y_2} d\ \cos\ k_{y_1}(b-2d) + \frac{k_{y_1}}{k_{y_2}}\frac{\epsilon_{r2}}{\epsilon_{req}}\ \cos\ k_{y_2} d. \tag{79}$$

$$\sin\ k_{y_1}(b-2d)$$

$$T_3 = \cos\ k_{y_2} d\ \cos\ k_{y_1}\ (b-2d)$$
$$-\frac{k_{y_2}}{k_{y_1}}\frac{\epsilon_{req}}{\epsilon_{r_2}}\ \sin\ k_{y_2} d\ .\ \sin\ k_{y_1}(b-2d). \tag{80}$$

The variation of the total relative power and the relative power in regions 1, 2 and 3 for some of the $LSE_{mn}$ and $LSM_{mn}$ modes are shown in Figs. 16.1 to 17.2 respectively.

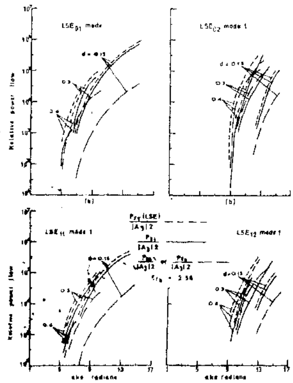

FIG. 16.1. Relative power flow in regions 1, 2 and 3 and total relative power flow vs. $ak_0$ for $LSE_{mn}$ mode.

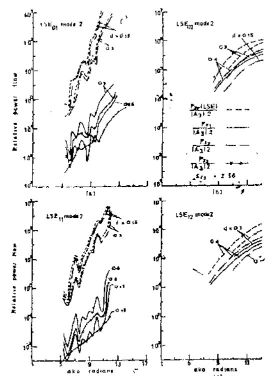

FIG. 16.2. Relative power flow in regions 1, 2 and 3 and total relative power flow vs. $ak_0$ for $LSE_{mn}$ mode 2.

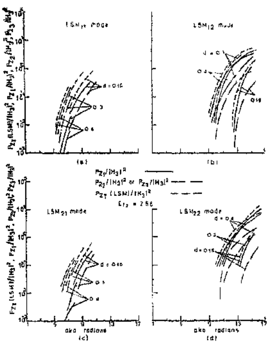

FIG. 17.1. Relative power flow in regions 1, 2 and 3 and total relative power flow vs. $ak_0$ for $LSM_{mn}$ mode 1.

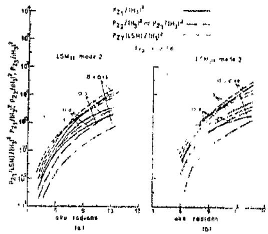

FIG. 17.2. Relative power flow in regions 1, 2 and 3 and total relative power flow vs. $ak_0$ for $LSM_{mn}$ mode 2.

## 14. Power loss and attenuation constants for $LSE_{mn}$ and $LSM_{mn}$ modes

There are two types of power losses, namely, (i) powei loss in the dielectric media and (ii) ohmic loss due to the finite conductivity of the metallic walls. Both these types of losses are calsulated to calculate the attenuation constant in the dielectric-lined waveguide.

In the previous sections it was assumed that the dielectric material used for the lining is perfect (zero conductivity) and the metallic wall of the waveguide is a perfect conductor (in future conductivity). However, in practice, the power loss in the dielectric-lined waveguide is caused by the finite value of the loss tangent of the material, and by the finite conductivity of the metal walls, and consequently, the axial propagation constant becomes complex.

In the presence of loss, the power transport along the waveguide decreases exponentially according to the factor exp $(-2a_z)$, where $a$ is the attenuation constant. If $P_0$ is the power flow at $z = 0$, when $P_z = P_0 \exp(-2a_z)$ is the power flow at $z = z$ in the $z$ direction. The rate of decrease of the power transport is then given by [14]

$$dP_z | d_z = P_t = -2a P_z. \tag{81}$$

If the relative permittivity of the dielectric lining is given by

$$\epsilon_r = \epsilon_r - j\, \epsilon_r' \tag{82}$$

where

$\epsilon_r'/\epsilon_r = \tan\,\delta,$

the power loss $P$ per unit length in the dielectric material is given by

$$P_d = \frac{1}{2} \iint_S |\mathbf{E}| \cdot |\mathbf{J}|\, da$$

$$= \frac{\omega\epsilon_0\,\epsilon_r'}{2} \iint_S \mathbf{E} \cdot \mathbf{E}^*\, da \tag{83}$$

where $\mathbf{J} = \sigma_{d_i}\mathbf{E} = \omega\epsilon_0\,\epsilon_r'\,\mathbf{E}$ the conduction current density

$\sigma_{d_i}$ = finite conductivity of the medium ($i = 1,2,3$ denoting the regions 1,2,3)

$S$ = cross-section of the guide transverse to the direction of propagation.

Equation (83) becomes

$$P_d = \frac{\sigma_{d_i}}{2} \iint_S (|E_{xi}|^2 + |E_{yi}|^2 + |E_{zi}|^2)\, dy\, dx \tag{84}$$

in the different regions 1,2,3,

where $\sigma_{d_i} = \omega\epsilon_0\,\epsilon_{r_i}\,\tan\,\delta_i$,

$\tan\,\delta_i$ = loss tangent of medium $i$ ($i = 1,2,3$).

If the dielectric lining is lossy and its dielectric constant is

$$\hat{\epsilon}_{r_2} = \epsilon_{r_2} - j\,\epsilon_{r_2}' \tag{85}$$

where $\tan\,\delta_2 = \epsilon_{r_2}'/\epsilon_{r_2}$, then the equivalent dielectric constant $\epsilon_{req}$ is also complex and is given by

$$\hat{\epsilon}_{req} = \epsilon_{req} - j\epsilon'_{req} \tag{86}$$

$$= \frac{a\,(\epsilon_{r_2} - j\epsilon_{r_2}')}{(a-2d)\left[\dfrac{2d}{(a-2d)} + \epsilon_{r_2} - j\,\epsilon_{r_2}'\right]} \tag{87}$$

(using eqns. (2) and (85)). Therefore

$$\epsilon_{req} = \frac{a\left[\epsilon_{r_2}\left(\dfrac{2d}{a\,.\,2d} + \epsilon_{r_2}\right) + \epsilon_{r_2}^2\tan\delta_2\right]}{(a-2d)\left[\left(\dfrac{2d}{a-2d} + \epsilon_{r_2}\right)^2 + \epsilon_{r_2}^2\tan^2\delta_2\right]} \tag{88}$$

and

$$\tan\,\delta_{eq} = \frac{\epsilon'_{req}}{\epsilon_{req}}$$

$$= \frac{a\left[\epsilon_{r_2}\tan\delta_2\left(\dfrac{2d}{a-2d} + \epsilon_{r_2}\right) - \epsilon_{r_2}^2\tan\delta_2\right]}{\epsilon_{req}\,(a-2d)\left[\left(\dfrac{2d}{a-2d} + \epsilon_{r_2}\right)^2 + \epsilon_{r_2}^2\tan\delta_2\right]} \tag{89}$$

As $\tan\delta_2 \to 0$, eqn. (88) reduces to eqn. (2). The total power loss $P_{d_{T(LSE)}}$ in the dielectric media for the $LSE_{mn}$ mode is the sum of the power losses $P_{d_1}$, $P_{d_2}$ and $P_{d3}$ in regions 1, 2 and 3 respectively. Hence

$$\begin{aligned} P_{d_T\,(LSE)} &= P_{d_1} + P_{d_2} + P_{d_3} \\ &= \tfrac{1}{2}\sigma_{d_1} \int_0^a \int_d^{(b-d)} (|E_{x_1}|^2 + |E_{y_1}|^2 + |E_{z_1}|^2)\, dy\, dx \\ &+ \tfrac{1}{2}\sigma_{d_2} \int_{(b-d)}^{b} (|E_{x_2}|^2 + |E_{y_2}|^2 + |E_{z_2}|^2)\, dy\, dx \\ &+ \tfrac{1}{2}\sigma_{d_3} \int_0^a \int_0^d (|E_{x_3}|^2 + |E_{y_3}|^2 + |E_{z_3}|^2)\, dy\, dx \end{aligned} \tag{90}$$

where $\sigma_{d_2} = \sigma_{d_3}$ is the finite conductivity of the dielectric regions 2 and 3, $\sigma_{d_1}$ is the finite conductivity of the equivalent dielectric region, and $\mu_r = 1$ for all the regions. Making use of eqns. (17), (18) and (19),

$$\begin{aligned} P_{dT\,(LSE)} = \frac{a^2\omega^2\mu_0^2}{2N_0}\left(\beta_{mn}^2 + \frac{m^2\pi^2}{a^2}\right)\Bigg[\sigma_{d_2}|A_3|^2\left(\frac{d}{2} - \frac{\sin^2 k_{y_2} d}{4k_{y_2}}\right) \\ + \sigma_{d_1}\Bigg\{|A_1|^2\left(\frac{(b-2d)}{2} - \frac{\sin 2k_{y_1}(b-2d)}{4k_{y_1}}\right) \\ + |B_1|^2\left(\frac{b-2d}{2} + \frac{\sin^2 k_{y_1}(b-2d)}{2k_{y_1}}\right) + (A_1B_1^* + A_1^* B_1) \\ \sin^2 k_{y_1}(b-2d)/2k_{y_1}\Bigg\} \\ + \sigma_{d_2}\Bigg\{|A_2|^2\left(\frac{d}{2} - \frac{\sin 2k_{y_2} d}{4k_{y_2}}\right) \\ + |B_2|^2\left(\frac{d}{2} + \frac{\sin 2k_{y_2} d}{4k_{y_2}}\right) \\ + (A_2B_2^* + A_2^* B_2)\frac{\sin^2 k_{y_2} d}{2k_{y_2}}\Bigg\}\Bigg] \end{aligned} \tag{91}$$

where the amplitude constants $A_1$, $A_2$, $B_1$ and $B_2$ are given in terms of $C_1$, $C_2$, $D_2$ and $D_2$ by the two equations:

$$\begin{aligned} C_k &= A_k \cos k_{y_k} y_k + B_k \sin k_{y_k} y_k \\ D_k &= B_k \cos k_{y_k} y_k - A_k \sin k_{y_k} y_k \end{aligned} \tag{92}$$

where $k = 1, 2$.

the attenuation constant $\alpha_{\bar{d}}$ for $LSE_{mn}$ mode can be calculated as

$$\alpha_{d\,(LSE)} = \frac{P_{d_T\,(LSE)}}{2\,P_{z_T\,(LSE)}} \text{ nepers per cm}$$

$$= \frac{8 \cdot 686\ P_{d_T\,(LSE)}}{2\,P_{z_T\,(LSE)}}\ db \text{ per cm} \tag{93}$$

where $P_{z_T\,(LSE)}$ is the power flow given by eqn. (74).

Due to the finite conductivity of the waveguide metallic wall also, the electromagnetic field is attenuated. The surface current density $\mathbf{J}_s$ in the metal wall is given by

$$\mathbf{J}_s = \mathbf{n} \times \mathbf{H}.$$

Hence the power loss per unit length of the metal wall is given by

$$P_m = \tfrac{1}{2}\ \mathrm{Re}\ Z_s \oint_{\text{wall}} \mathbf{J}_s \,.\, \mathbf{J}_s^*\ dl$$

$$= \tfrac{1}{2} R_s \oint_{\text{wall}} \mathbf{H}_t \cdot \mathbf{H}_t^*\, dl \tag{94}$$

where

$$Z_s = \frac{1+j}{\delta} = R_s + j\,X_s \tag{95}$$

$\sigma_\omega$ being the finite conductivity of the metallic wall, $Z_s$ the surface impedance of the metal wall, and $R_s = 1/\sigma_\omega \delta$ is the surface resistance of the metal wall, and $\delta = (2/\omega\mu_0\sigma_\omega)^{1/2}$ is the skin depth. Hence

$$R_s = \left(\frac{\omega\mu_0}{2}\right)^{1/2}.$$

Hence the total power dissipated per unit length in the metal walls for the $\mathrm{LSE}_{mn}$ mode is

$$P_{mT\,(LSE)} = \tfrac{1}{2}\ R_s \oint_{\text{side walls}} (|\,H_{y_i}\,|^2 + |\,H_{z_i}\,|^2)\ dy$$

$$+ \tfrac{1}{2} R_s \oint_{\text{top and bottom walls}} (|\,H_{x_i}\,|^2 + |\,H_{z_i}\,|)^2\ dx \tag{96}$$

$(i = 1,2,3)$

$$= \frac{R_s}{2}\left\{a\,|\,k_{y_2}\,|^2\left[\frac{\beta_{mn}^2}{N_0} + \frac{m^2\,\pi^2}{2a^2}\right](|\,A_3\,|^2 + |\,A_2 \cos k_{y_2}\,d - B_2 \sin k_{y_2}\,d\,|^2)\right.$$

$$+ 2\left[\beta_{mn}^2 + \frac{m^2\,\pi^2}{a^2}\right]^2 (|\,A_3\,|^2)\left(\frac{d}{2} - \frac{\sin k_{y_2}\,d}{4k_{y_2}}\right)$$

$$+ |\,A_1\,|^2\left(\frac{(b-2d)}{2}\ \frac{\sin\ 2k_{y_1}(b-2d)}{4k_{y_1}}\right)$$

$$+ |\,B_1\,|^2\left(\frac{b-2d}{2} + \frac{\sin 2k_{y_1}(b-2d)}{4k_{y_1}}\right) + |\,A_2\,|^2\left(\frac{d}{2} - \frac{\sin 2k_{y_2}\,d}{4k_{y_2}}\right)$$

$$+ |\,B_2\,|^2\left(\frac{d}{2} + \frac{\sin\ 2k_{y_2}d}{4k_{y_2}}\right) + (A_1 B_1^* + A_1^* B_1)\,\frac{\sin^2\ k_{y_1}(b-2d)}{4k_{y_1}}$$

$$+ (A_2 B_2^* + A_2^*\,B_2)\ \frac{\sin^2 k_{y_2}d}{2k_{y_2}} + 2\beta_{mn}^2\,(|\,A_3\,|^2\,|\,k_{y_2}\,|^2)$$

$$\times\left(\frac{d}{2}+\frac{\sin 2k_{y_2}d}{4k_{y_2}}\right)+|A_1|^2|k_{y_1}|^2\left(\frac{(b-2d)}{2}+\frac{\sin 2k_{y_1}(b-2d)}{4k_{y_1}}\right)$$

$$+|B_1|^2|k_{y_1}|^2\left(\frac{(b-2d}{2}-\frac{\sin 2k_{y_1}(b-2d)}{4k_{y_1}}\right)+|A_2|^2|k_{y_2}|^2$$

$$\times\left(\frac{d}{2}+\frac{\sin 2k_{y_2}d}{4k_{y_2}}\right)+|B_2|^2|k_{y_2}|^2\left(\frac{d}{2}-\frac{\sin 2k_{y_2}d}{4k_{y_2}}\right)$$

$$-(A_1B_1^*+A_1^*B_1)\ |k_{y_1}|^2\frac{\sin^2 k_{y_1}(b-2d)}{2k_{y_1}}$$

$$-\left(A_2B_2^*+A_2^*B_2)\ |k_{y_2}|^2\frac{\sin^2 k_{y_2}d}{2k_{y_2}}\right)\Bigg\} \tag{97}$$

where $A_1$, $B_1$, $A_2$, $B_2$ are given by eqns. (92) and $A_3 = C_3$, and $B_3 = D_3$, and $A_1$, $A_2$, $B_1$ and $B_2$ are related to $A_3$ by the following equations :

$$B_1 = A_3 \sin k_{y_2}d = A_3F_1 \tag{98}$$

$$A_1 = A_3\frac{k_{y_2}}{k_{y_1}}\cos k_{y_2}d = A_3E_1 \tag{99}$$

$$B_2 = A_3\left[\frac{k_{y_2}}{k_{y_1}}\cos k_{y_2}d\sin k_{y_1}(b-2d)+\sin k_{y_2}d\cos k_{y_1}(b-2d)\right] = A_3F_2 \tag{100}$$

$$A_2 = A_3\Big[\cos k_{y_2}d\cos k_{y_1}(b-2d)$$

$$-\frac{k_{y_1}}{k_{y_2}}\sin k_{y_2}d\sin k_{y_1}(b-2d)\Big] = A_3E_2. \tag{101}$$

The attention constant $a_{m(LSE)}$ for $\mathrm{LSE}_{mn}$ mode is given by

$$a_{m(LSE)} = \frac{P_{mT(LSE)}}{2P_{zT(LSE)}}\text{ nepers per cm}$$

$$= \frac{8\cdot686\ P_{mT(LSE)}}{2P_{zT(LSE)}}\ db\text{ per cm.} \tag{102}$$

The total attenuation constant $a_{T(LSE)}$ for $\mathrm{LSE}_{mn}$ mode is given by

$$a_{d(LSE)} + a_{m(LSE)} \tag{103}$$

using eqns. (93) and (102).

Similarly the total attenuation constant $a_{T(LSM)}$ for $\mathrm{LSM}_{mn}$ modes is given by

$$a_{T(LSM)} = a_{d(LSM)} + a_{m(LSM)} \tag{104}$$

where

$$a_{d(LSM)} = \frac{P_{dT(LSM)}}{2P_{zT(LSM)}}\text{ nepers per cm}$$

$$= 8\cdot686\,\frac{P_{dT(LSM)}}{2P_{zT(LSM)}} \tag{105}$$

$P_{dT(LSM)}$

$$= \frac{\sigma d_1}{4} a \left[\beta_{mn}^2 + \frac{m^2\pi^2}{a^2}\right]\Bigg[|k_{y_1}|^2 \Bigg\{|G_1|^2 \frac{b-2d}{2} - \frac{\sin 2k_{y_1}(b-2d)}{4k_{y_1}}$$

$$+ |H_1|^2 \left(\frac{b-2d}{2} - \frac{\sin 2k_{y_1}(b-2d)}{4k_{y_1}}\right) - (G_1H_1^* + G_1^* H_1)$$

$$\times \frac{\sin^2 k_{y_1}(b-2d)}{2k_{y_1}}\Bigg\}\Bigg] + \left(\beta_{mn}^2 + \frac{m^2\pi^2}{a^2}\right)\Bigg\{|G_1|^2\left(\frac{b-2d}{2} - \frac{\sin 2k_{y_1}(b-2d)}{4k_{y_1}}\right)$$

$$+ |H_1|^2 \left(\frac{b-2d}{2} + \frac{\sin 2k_{y_1}(b-2d)}{4k_{y_1}}\right) + (G_1H_1^* + G_1^*H_1)$$

$$\times \frac{\sin^2 k_{y_1}(b-2d)}{2k_{y_1}}\Bigg\} + \frac{\sigma d_2}{4} a \left[\beta_{mn}^2 + \frac{m^2\pi^2}{a^2}\right]\Bigg[|k_{y_2}|^2 \Bigg\{|G_2|^2$$

$$\times \left(\frac{d}{2} + \frac{\sin 2k_{y_2}d}{4k_{y_2}}\right) + |H_2|^2\left(\frac{d}{2} - \frac{\sin 2k_{y_2}d}{4k_{y_2}}\right) - (G_2H_2^* + G_2^*H_2)\frac{\sin^2 k_{y_2}d}{2k_{y_2}}\Bigg\}$$

$$+ \left(\beta_{mn}^2 + \frac{m^2\pi^2}{a^2}\right)\Bigg\{|G_2|^2 \left(\frac{d}{2} - \frac{\sin 2k_{y_2}d}{4k_{y_2}}\right) + |H_2|^2\left(\frac{d}{2} + \frac{\sin 2k_{y_2}d}{4k_{y_2}}\right)$$

$$+ (G_2H_2^* + G_2^* H_2)\frac{\sin^2 k_{y_2}d}{2k_{y_2}}\Bigg\}\Bigg] + \frac{\sigma d_2}{4}|H_3|^2\left(\beta_{mn}^2 + \frac{m^2\pi^2}{a^2}\right)$$

$$\times \left[|k_{y_2}|^2\left(\frac{d}{2} - \frac{\sin 2k_{y_2}d}{4k_{y_2}}\right) + (\beta_{mn}^2 + \frac{m^2\pi^2}{a^2})\left(\frac{d}{2} + \frac{\sin 2k_{y_2}d}{4k_{y_2}}\right)\right] \tag{106}$$

and $P_{zT(LSM)}$ is given by eqn. (78).

and

$$\alpha_{m\,(LSM)} = \frac{P_{mT(LSM)}}{2P_{zd\,(LSM)}} \text{ nepers per cm}$$

$$= 8 \cdot 686 \frac{P_{mT(LSM)}}{2P_{zT\,(LSM)}}\, db \text{ per cm} \tag{107}$$

where

$P_{mT(LSM)}$

$$= \frac{R_s}{2}\left[\omega^2 \epsilon_0^2 \frac{a}{2}\left(\beta_{mn}^2 + \frac{m^2\pi^2}{a^2}\right)\epsilon_{r2}^2 \{|H_3|^2 + |G_2 \sin k_{y_2}d + H_2 \cos k_{y_2}d|^2\}\right.$$

$$+ 2\omega^2 \epsilon_0^2 \frac{m^2\pi^2}{a^2}\Bigg\{\epsilon_{r_2}^2 |H_3|^2\left(\frac{d}{2} + \frac{\sin 2k_{y_2}d}{4k_{y_2}}\right) + \epsilon_{req}^2 |G_1|^2$$

$$\times \left(\frac{b-2d}{2} - \frac{\sin 2k_{y_1}(b-2d)}{4k_{y_1}}\right) + \epsilon_{req}^2 |H_1|^2 \left(\frac{(b-2d}{2}\frac{\sin 2k_{y_1}(b-2d)}{4k_{y_1}}\right)$$

$$+ \epsilon^2_{req} (G_1 H_1^* + G_1^* H_1) \frac{\sin^2 k_{y_1}(b-2d)}{2k_{y_1}} + \epsilon_{r2}^2 \mid G_2 \mid^2 \left(\frac{d}{2} - \frac{\sin 2k_{y_2}d}{2k_{y_2}}\right)$$

$$+ \epsilon_2^2 \mid H_2 \mid^2 \left(\frac{d}{2} + \frac{\sin 2k_{y_2}d}{4k_{y_2}}\right) + \epsilon_{r2}^2 (G_2 H_2^* + G_2^* H_2) \frac{\sin^2 k_{y_2}d}{2k_{y_2}}\Big\}\Big] \qquad (108)$$

The total attenuation constants for different LSE and LSM modes *vs.* $ak_0$ are shown in Figs. 18 and 19 respectively.

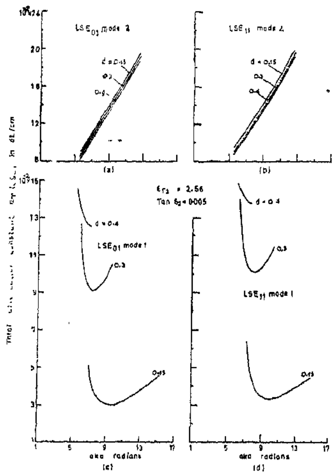


FIG. 18.0. Total attenuation constant $a_t$ (LSE) vs. $ak_0$.

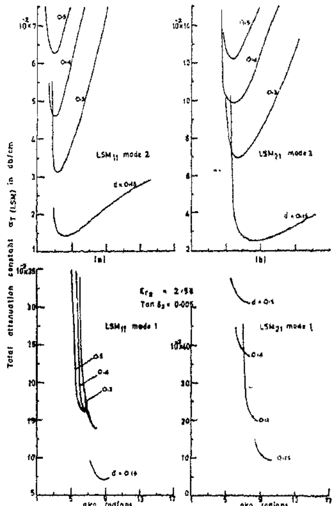


FIG. 19.0. Total attenuation constant $a_t$ (LSM) vs. $ak_0$.

## 15. Power handling capacity

The power handling capacity of the dielectric-lined waveguide is calculated by using the following two methods:

(i) Breakdown electric field.

(ii) Temperature rise in the dielectric.

The power handling capacity calculated by the first method determines the power capabilities within the limits of the electric breakdown of the dielectric medium free from obstacles and discontinuities[3,15]. This provides the maximum transmissible power on the basis of the highest allowable electric field strength.

However, the power transmission through the dielectric materials is accompanied by heating, and since the dielectric materials soften at high temperatures, the maximum possible degree of overheating has to be determined. This is done by the second method which determines the maximum power handling capacity by the dielectric-lined waveguide.

## 15.1. *Breakdown electric field method*

The maximum transmissible power in the dielectric-lined waveguide is calculated by knowing the highest permissible value of the electric field which causes the breakdown at the interfaces of the equivalent dielectric and the dielectric material.

For $LSE_{mn}$ modes, in the case of the mode for which $m = 0$, it is evident from the field components of various regions (eqns. (17) to (22)) that only the $E_x$ component exists and therefore the maximum value of $E$ at the interface of the two media will decide the dielectric breakdown. At $y = y_1$, with the aid of eqn. (17), the maximum electric field is given by

$$E_{x_1(\max)} = \omega\mu_0\mu_r\beta_{mn}D_1 \tag{109}$$

and using eqn. (98), we have

$$E_{x_1(\max)} = A_3\omega\mu_0\mu_r\beta_{mn}\sin k_{y_2}d,$$

so that

$$A_3 = \frac{E_{x_1(\max)}}{\omega\mu_0\mu_r\beta_{mn}\sin k_{y_2}d} = C_3. \tag{110}$$

The breakdown electric field strength for air is $2 \cdot 9 \times 10^4$ volts/cm. If the dielectric lining of the waveguide is thin, the thickness of the equivalent dielectric region will be large and the dielectric density small. In the limiting case when $d \to 0$, the waveguide is completely filled with air ($\epsilon_r = 1$), and its dielectric breakdown is $2 \cdot 9 \times 10^4$ volts/cm under normal temperature and pressure.

Considering the intrinsic breakdown of the dielectric with pulses of short duration and at sufficiently low temperatures where heating effects are avoided, the maximum electric field that can be applied to dielectric materials depends mainly on the discharge inception field and thus on the permittivity of the material. Therefore since $\epsilon_{req} > 1$, the equivalent dielectric material withstands a greater breakdown field than air ($\epsilon_r = 1$).

The breakdown field for the equivalent dielectric material can also be assumed to be $2 \cdot 9 \times 10^4$ volts/cm at normal temperature and pressure. Hence

$$E_{x_1(\max)} = 2 \cdot 9 \times 10^4 \text{ volts/cm.} \tag{111}$$

Therefore from eqn. (110), we have

$$A_3 = \frac{2 \cdot 9 \times 10^4 \text{ volts/cm}}{\omega\mu_0\beta_{mn} \sin k_{y_2}d} \tag{112}$$

(putting $\mu_r = 1$).

Substituting eqn. (112) in eqn. (74), the maximum power handling capacity for the $LSE_{on}$ modes can be calculated.

The variation of the maximum power handling capacity $P_{zT(LSE_{on})\,max}/a^2$ with frequency and dielectric lining thickness $d$ for some $LSE_{on}$ modes of type 1 are shown in Fig. 20 for $\epsilon_{r_2} = 2 \cdot 08$ and $\epsilon_{r_2} = 2 \cdot 56$.

For $LSE_{mn}$ modes for which $m > 0$, there are two electric field components $E_x$ and $E_z$. Assuming the dielectric breakdown at the interface $y = d$, it is necessary to find the greater of the two field components $E_x$ and $E_z$. The component thus found decides the breakdown field of the equivalent dielectric material.

From eqns. (17) and (19), and from the boundary conditions (23) to (26), it can be seen that at $y = d = y_1$,

$$E_{x_1} = \omega\mu_0\mu_r\beta_{mn}A_3 \sin k_{y_2}d \cos \frac{m\pi}{a} x \tag{113}$$

$$E_{z_1} = j\omega\mu_0\mu_r \frac{m\pi}{a} A_3 \sin k_{y_2}d \sin \frac{m\pi}{a} x. \tag{114}$$

$E_{x_1}$ is maximum at $x = 0$ and at $x = a/m$ along the interface $y = d$.

Therefore

$$E_{x_1\,(max)} = \omega\mu_0\mu_r\beta_{mn}A_3 \sin k_{y_2}d \tag{115}$$

and $E_{z_1}$ is maximum at $x = a/2m$ along the interface. This gives

$$E_{z_1\,(max)} = j\omega\mu_0\mu_r \frac{m\pi}{a} A_3 \sin k_{y_2}d. \tag{116}$$

Comparing eqns. (115) and (116), it can be seen that $E_{x_1\,(max)} > E_{z_1\,(max)}$ when $\beta_{mn}a > m\pi$. (117)

Hence $E_{x_1\,(max)} = 2 \cdot 9 \times 10^4$ volts/cm (118)

which again gives

$$A_3 = \frac{E_{x_1\,(max)}}{\omega\mu_0\beta_{mn} \sin (k_{y_2}d)} \tag{119}$$

Equation (119) can be used in eqn. (74) to find the maximum power handling capacity for the $LSE_{mn}$ $(m > 1)$ modes.

The variations of maximum power handling capacity $P_{zT\,(LSE_{mn})\,max}/a^2$ with frequency and dielectric lining thickness for $LSE_{11}$ and $LSE_{12}$ modes of type 1 are shown in Fig. 21.

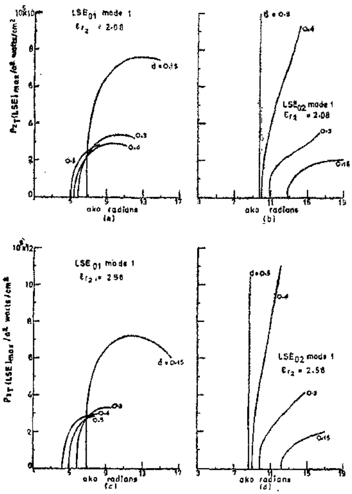


FIG. 20. Maximum power handling capacity vs. $ak_0$ for $LSE_{on}$ (n = 1 and 2) mode 1.

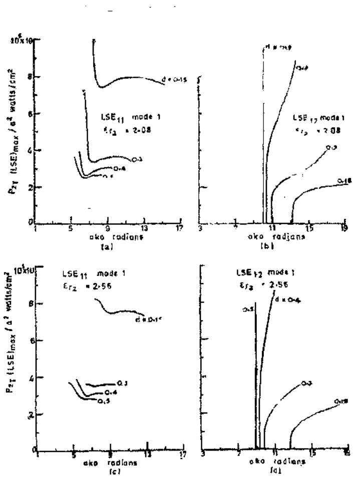


FIG. 21. Maximum power handling capacity vs. $ak_0$ for $LSE_{ln}$ (n = 1 and 2) mode 1.

For $LSM_{mn}$ modes the electric field components at $y = d = y_1$ can be written as follows:

$$E_{x_1} = -H_z k_{y_2} \frac{m\pi}{a} \sin k_{y_2} d \cos \frac{m\pi}{a} x \tag{120}$$

$$E_{y_1} = H_3 \frac{\epsilon_{r_2}}{\epsilon_{\text{req}}} \left( \beta_{mn}^2 + \frac{m^2 \pi^2}{a^2} \right) \cos k_{y_2} d \frac{\sin m\pi}{z} x \tag{121}$$

$$E_{z_1} = jH_3 k_{y_2} \beta_{mn} \sin k_{y_2} y \frac{\sin m\pi}{a} x. \tag{122}$$

When $x = 0$ or $a$

$$(E_{x_1})_{\max} = H_3 \frac{m\pi}{a} k_{y_2} \sin k_{y_2} d. \tag{123}$$

When $x = a/2m$,

$$(E_{y_1})_{\max} = H_3 \frac{\epsilon_{r_2}}{\epsilon_{\text{req}}} \left( \beta_{mn}^2 + \frac{m^2 \pi^2}{a^2} \right) \cos k_{y_2} d \tag{124}$$

and

$$(E_{y_1})_{\max} = j\beta_{mn} H_3 k_{y_2} \sin k_{y_2} d. \tag{125}$$

Therefore $E_{y_1(\max)} > E_{z_1(\max)} > E_{x_1(\max)}$

when $a\beta_{mn} > m\pi$.

Hence the maximum power handling capacity is calculated by putting $E_{y_1(\max)} = 2\cdot 9 \times 10^4$ volts/cm which gives

$$H_3 = \frac{\epsilon_{req}\, a^2\, 2\cdot 9 \times 10^4 \text{ volts/cm}}{\epsilon_{r_2}(a^2 \beta_{mn}^2 + m^2 \pi^2) \cos k_{y_2} d}. \tag{126}$$

Using eqn. (126) in eqn. (78), the maximum power handling capacity for $LSM_{mn}$ modes is found. The variation of $P_{zT\,(LSM)\,(\max)}/a^2$ with frequency and dielectric lining thickness for some of the $LSM_{mn}$ modes of type 2 are shown in Fig. 22.

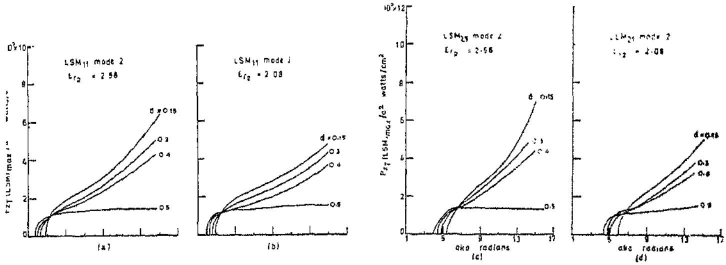


FIG. 22. Maximum power handling capacity vs. $ak_0$ for $LSM_{m1}$ (m = 1 and 2) mode 2.

### 15.2. *Method using temperature raise in the dielectric*

The power lost per unit length is expressed as follows:

$$\frac{dP_z}{dz} = \frac{2aP_z}{8\cdot 686} \tag{123}$$

where $P_z$ is the axial power flow and $a$ is the attenuation constant in decibels per unit length.

The heat is mostly developed in the dielectric itself as the field is concentrated in the dielectric materials of higher permittivity at high frequencies.

The general equation of heat conduction is given by [24, 25]

$$\frac{dQ}{dt} = k_h \frac{A_1}{d_0}(T_1 = T_2) \text{ kilocalories per hour} \tag{124}$$

where $dQ/dt$ = rate of heat flow

$A_1$ = surface area at right angles to the heat flow in $(\text{cm})^2$

$d_0$ = length of the conducting path in cm

$k_h$ = thermal conductivity of the dielectric in kilocalories/hour (cm) (°C).

$T_1$ and $T_2$ are temperatures in °C on the two faces of the interface between two dielectrics (in this case $T_1$ is in air and $T_2$ is in the dielectric lining).

The thermal resistance $R_T$ is defined as

$$R_T = \frac{d_0}{k_h A_i}. \tag{125}$$

The power loss per unit length is given by [24]

$$\frac{dP_z}{dz} = 1 \cdot 1633 \frac{dQ}{dt} \text{ in watts} \tag{126}$$

(1 kilocal/hour = 1·1633 watts)

From eqns. (126) and (123), we obtain

$$\frac{dQ}{dt} = \frac{aP_z}{5 \cdot 037}. \tag{127}$$

The following assumptions are made for calculating the average power flow based on the softening temperature of the dielectric lining material:

(i) that there is no air gap between the dielectric lining and the metal wall; and

(ii) the heat transfer by convection from the metallic surface is negligible.

Considering that the heat developed in the dielectric flows through the outer surface of the dielectric lining uniformly, the total rate of heat flow [25] is:

$$\frac{dQ}{dt} \frac{(T_1 - T_2) + (T_2 - T_3)}{R_d + R_m} = \frac{T_1 - T_3}{R_d + R_m} \tag{128}$$

where

$T_1 - T_2$ = temperature difference between the two faces of the dielectric lining in °C

$T_2 - T_3$ = temperature difference between the two faces of the metallic wall

$R_d = \left(\frac{d}{k_d A_d}\right)$ = the thermal resistance of the dielectric

$k_d$ = the thermal conductivity of the dielectric lining in kilocal (hour) (cm) (°C)

$A_d$ = average dielectric area in $(\text{cm})^2$

$d$ = dielectric thickness in cm

$R_m = \left(\frac{d_1}{k_m A_m}\right)$ = the thermal resistance of the metal surface

$k_m$ = the thermal conductivity of the metal in kilocal/(hr) (cm) (°C)

$A_m$ = average metallic area in $(\text{cm})^2$

$d_1$ = metallic wall thickness in cm

Equation (128) can be written as

$$(T_1 - T_3) = \frac{dQ}{dt} R_d + \frac{dQ}{dt} R_m \tag{129}$$

which for $LSE_{mn}$ mode becomes

$$(T_1 - T_3) = \frac{P_{zT\,(LSE)}}{5 \cdot 037} \left( \frac{d\alpha_d(\mathrm{LSE})}{K_d A_d} + \frac{d_1 \alpha_{m\,(LSE)}}{k_m A_m} \right) \tag{130}$$

where

$\alpha_{d\,(LSE)}$ = dielectric attenuation in db/cm given by eqn. (93)

$\alpha_{m\,(LSE)}$ = metallic attenuation in db/cm given by eqn. (102)

The average dielectric area in $(\mathrm{cm})^2$ is

$$A_d = \frac{A_{a_1} + A_{d_1}}{2} = 2\,(a + b - 2d) \tag{131}$$

and the average metallic area in $(\mathrm{cm})^2$ is

$$A_m = \frac{A_{d_1} + A_{m_1}}{2} = 2\,(a + b + 2d_1) \tag{132}$$

where

$A_{a_1}$ = surface area of the air-dielectric boundary $= 2\,(a + b - 4d)$ in $(\mathrm{cm})^2$

$A_{d_1}$ = surface area of the dielectric-metal boundary $= 2\,(a + b)$ in $(\mathrm{cm})^2$

and

$A_{m_1}$ = surface area of the outer metal surface

$= 2\,(a + b + 4d_1)$ in $(\mathrm{cm})^2$.

Then eqn. (130) can be written as

$$P_{zT\,(LSE)} = \frac{5 \cdot 037\,(T_1 - T_3)}{\dfrac{d\alpha_{d\,(LSE)}}{K_d A_d} + \dfrac{d_1 \alpha_{m\,(LSE)}}{k_m A_m}}\,. \tag{133}$$

Maximum transmissible power limited by the dielectric overheating in the dielectric-lined waveguide is given by:

$$P'_{zT\,(LSE)\,\max} = \frac{5 \cdot 037\,(T - T_3)_{\max}}{\dfrac{d\alpha_{d\,(LSE)}}{K_d A_d} + \dfrac{d_1 \alpha_{m\,(LSE)}}{K_m A_m}} \tag{134}$$

where

$(T_1 - T_3)_{\max}$ = maximum temperature difference between the inner dielectric surface and the outer metallic surface

Similarly for LSM modes,

$$P'_{zT\,(LSM)\max} = \frac{5 \cdot 037\,(T_1 - T_3)_{\max}}{\dfrac{d\alpha_{d\,(LSM)}}{k_d A_d} + \dfrac{d_1 \alpha_{m\,(LSM)}}{k_m A_m}} \tag{135}$$

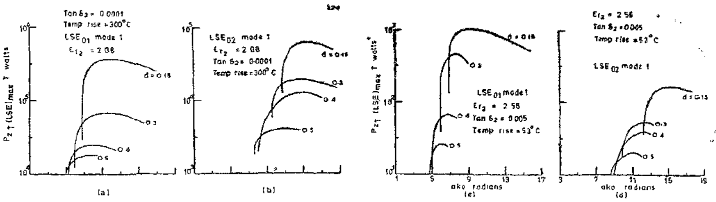


FIG. 23. Maximum power handling capacity (Temp. rise) vs. $ak_0$ for $LSE_{0n}$ ($n = 1$ and 2) mode 1.

where $a_{d\,(\text{LSM})}$ and $a_{m(\text{LSM})}$ are given by eqns. (103) and (107) respectively. The power handling capacity has been calculated in the two cases of dielectric lining, *viz.*, perspex and teflon for both LSE and LSM modes using eqns. (134) and (135). The heat conductivity $K_d$ for perspex, teflon and brass are taken to be equal to $0 \cdot 1116 \times 10^{-2}$ kilocal/(hr) (cm) (° C), $0 \cdot 1666 \times 10^{-2}$ kilocal/(hr) (cm) (° C), and $0 \cdot 9360$ kilocal/(hr) (cm) (° C) respectively. The softening temperature $T_1$ for perspex and teflon are 78° C and 327° C respectively. The ambient temperature $T_3$ of the guide wall is taken to be 25° C, and the metallic wall thickness is $d_1 = 0 \cdot 127$ cm. The variations of power handling capacity $P'_{zT(\text{LSE})\,\max}$ with frequency and dielectric lining thickness are shown in Figs. 23 and 24 for two values $2 \cdot 08$ and $2 \cdot 56$ of the relative dielectric constant for some of the $\text{LSE}_{mn}$ modes. Fig. 25 shows the variations of $P_{zT(\text{LSM})\,\max}$ with frequency and $d$ for some $\text{LSM}_{mn}$ modes of type 2.

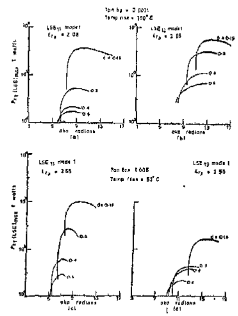

FIG. 24. Maximum power handling capacity (Temp. rise) vs. $ak_0$ for $\text{LSE}_{1n}$ ($n = 1$ and 2) mode 1.

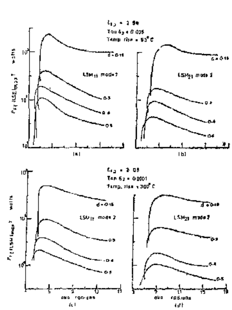

FIG. 25. Maximum power handling capacity (Temp. rise) vs. $ak_0$ for $\text{LSM}_{1n}$ ($m = 1$ and 2) mode 2.

## 16. Experimental work

An experimental study of the following has been done:

(i) Guide wavelength of $LSM_{11}$ mode type 2 at X-band (8·0–12·4 GHz);
Ku-band (12·4–18·0 GHz); and
Ku-band (26·5–40·0 GHz)

(ii) Cut-off frequency of the $LSM_{11}$ mode type 2.

The waveguide used is an X-band ($a = 2{\cdot}286$ cm, $b = 1{\cdot}016$ cm) slotted line-section with uniform dielectric lining on the inside on all four sides with perspex or teflon of different thicknesses.

Tables I and II give the frequency-guide wavelength characteristics in X- and Ku-bands respectively.

Table III gives the cut-off frequency for $LSM_{11}$ mode type 2 for perspex and teflon for two dielectric coating thicknesses.

## 17. Discussion

### 17.1. *The validity of the theory*

The approximate theory for the dielectric-lined rectangular waveguide has been derived by using the concept of the equivalent dielectric constant as given by eqns. (1) and (2). The experimental verification of the theoretical values of the guide wavelength and cut-off frequency proves the accuracy of the approximate theory.

### 17.2. *The characteristic equation*

The characteristic equation for $LSE_{mn}$ modes as given by eqn. (34) reduces to

$$\tan (k_{y_1} b) = 0 \quad \text{or} \quad k_{y_1} = \frac{n\pi}{b} \tag{136}$$

when $d = 0$ for the air-filled waveguide so that $\epsilon_{req} = 1$ and

$$\beta_{mn}^2 = k_0^2 - \frac{m^2 \pi^2}{a^2} - \frac{n^2 b^2}{b^2} \tag{137}$$

(from eqn. (54)).

which is satisfied by the $TE_{mn}$ and $TM_{mn}$ modes of the air-filled waveguide.

When the waveguide is completely filled with the dielectric material ($\epsilon_{r_2}$), *i.e.*, when $d = b/2$, eqn. (34) reduces to

$$2 \tan \left( k_{y_2} \frac{b}{2} \right) = 0 \text{ or}$$

$$k_{y_2} = 2n\pi/b \tag{138}$$

**Table I**

**Frequency-guide wavelength characteristics**

Frequency : *X*-band (8·0–12·4 GHz)

| Frequency in GHz | Theoretical | g in cm | | | Measured g in cm |
|---|---|---|---|---|---|
| | $LSM_{11}$ | | $LSM_{21}$ | | |
| | Mode 1 | Mode 2 | Mode 1 | Mode 2 | |
| (*a*) $\epsilon_{r_2} = 2\cdot56$; $d = 0\cdot15$ cm | | | | | |
| 8·3594 | .. | 4·2799 | .. | .. | 4·5600 |
| 9·4093 | .. | 3·4898 | .. | .. | 3·6400 |
| 10·4493 | .. | 2·9744 | .. | .. | 3·100 |
| 11·4942 | .. | 2·6045 | .. | 16·0050 | 2·7400 |
| (*b*) $\epsilon_{r_2} = 2\cdot08$; $d = 0\cdot15$ cm | | | | | |
| 8·3594 | .. | 4·4828 | .. | .. | 4·700 |
| 9·4033 | .. | 3·6307 | .. | .. | 3·800 |
| 10·4433 | .. | 3·0843 | .. | .. | 3·200 |
| 11·4942 | .. | 2·6961 | .. | .. | 2·800 |
| (*c*) $\epsilon_{r_2} = 2\cdot08$; $d = 0\cdot2$ cm | | | | | |
| 8·3594 | .. | 4·2960 | .. | .. | 4·36 |
| 9·4093 | .. | 3·4467 | .. | .. | 3·54 |
| 10·4493 | .. | 2·8620 | .. | .. | 2·96 |
| 11·4942 | .. | 2·4813 | .. | .. | 2·60 |
| (*d*) $\epsilon_{r_2} = 2\cdot56$; $d = 0\cdot3$ cm | | | | | |
| 8·3594 | .. | 3·3383 | .. | .. | 3·62 |
| 9·4093 | .. | 2·8041 | .. | .. | 3·04 |
| 10·4493 | .. | 2·4289 | .. | 6·2043 | 2·58 |
| 11·4942 | .. | 2·1475 | .. | 3·6930 | 2·32 |
| (*e*) $\epsilon_{r_2} = 2\cdot08$; $d = 0\cdot03$ cm | | | | | |
| 8·3594 | .. | 3·6523 | .. | .. | 3·95 |
| 9·4093 | .. | 3·0431 | .. | .. | 3·26 |
| 10·4493 | .. | 2·6254 | .. | 25·28 | 2·90 |
| 11·4942 | .. | 2·3166 | .. | 4·8328 | 2·50 |

**Table II**

**Frequency-guide wavelength characteristics**

Frequency: Ku-band (12·4–18·0 GHz)

| Frequency in GHz | Theoretical $g$ in cm LSM$_{11}$ Mode 1 | LSM$_{11}$ Mode 2 | LSM$_{21}$ Mode 1 | LSM$_{21}$ Mode 2 | Measured in $g$ cm |
|---|---|---|---|---|---|
| (a) $\epsilon_{r_2} = 2{\cdot}56$; $d = 0{\cdot}15$ cm | | | | | |
| 13·6107 | .. | 2·0994 | .. | 3·4633 | 2·180 |
| 14·6577 | .. | 1·9169 | .. | 2·7881 | 2·000 |
| 15·7077 | 4·2022 | 1·7643 | .. | 2·3720 | 1·820 |
| 16·7517 | 2·2805 | 1·6345 | .. | 2·0815 | 1·680 |
| 17·7956 | 2·2991 | 1·5224 | 4·6769 | 1·8635 | 1·560 |
| (b) $\epsilon_{r_2} = 2{\cdot}08$; $d = 0{\cdot}15$ cm | | | | | |
| 13·6107 | .. | 2·1708 | .. | 3·8158 | 2·24 |
| 14·6577 | .. | 1·9824 | .. | 3·0022 | 2·02 |
| 15·7077 | 5·2790 | 1·8254 | .. | 2·5271 | 1·84 |
| 16·7517 | 3·2831 | 1·6923 | .. | 2·2050 | 1·72 |
| 17·7956 | 2·5513 | 1·5777 | 9·9442 | 1·9678 | 1·58 |
| (c) $\epsilon_{r} = 2{\cdot}08$; $d = 0{\cdot}2$ cm | | | | | |
| 13·6107 | .. | 2·0612 | .. | 2·9612 | 2·14 |
| 14·6577 | .. | 1·8814 | .. | 2·7612 | 1·92 |
| 15·7077 | 6·52 | 1·7216 | .. | 2·4212 | 1·76 |
| 16·7517 | 3·92 | 1·6624 | .. | 2·0312 | 1·68 |
| 17·7956 | 2·86 | 1·4324 | .. | 1·7616 | 1·48 |
| (d) $\epsilon_{r_2} = 2{\cdot}56$; $d = 0{\cdot}3$ cm | | | | | |
| 13·6107 | 3·4838 | 1·7478 | .. | 2·3323 | 1·84 |
| 14·6577 | 2·4869 | 1·5994 | 7·4171 | 2·0104 | 1·69 |
| 15·7077 | 2·0119 | 1·4739 | 3·1080 | 1·7766 | 1·48 |
| 16·7517 | .. | 1·3662 | .. | 1·5967 | 1·37 |
| 17·7956 | .. | 1·2726 | .. | 1·4525 | 1·34 |
| (e) $\epsilon_{r_2} = 2{\cdot}08$; $d = 0{\cdot}3$ cm | | | | | |
| 13·6107 | 6·6017 | 1·8844 | .. | 2·6911 | 1·94 |
| 14·6577 | 3·3748 | 1·7257 | .. | 2·2806 | 1·76 |
| 15·7077 | 2·5194 | 1·5922 | 8·4446 | 1·9962 | 1·61 |
| 16·7517 | 2·0755 | 1·4781 | 3·3585 | 1·7840 | 1·49 |
| 17·7956 | 1·7911 | 1·3792 | 2·4383 | 1·6176 | 1·39 |

**Table III**

**Cut-off frequency for $LSM_{11}$ mode type 2**

| Material of lining | Thickness of lining in cm | Theoretical cut-off frequency of $LSM_{11}$ mode 2 in GHz | Measured cut-off frequency in GHz |
|---|---|---|---|
| Perspex ($\epsilon_{r_2} = 2{\cdot}56$) | 0·15 | 5·9285 | 5·60 |
| Perspex | 0·30 | 5·5447 | 5·20 |
| Teflon | 0·20 | 5·7420 | 5·50 |
| Teflon | 0·30 | 5·38 | 5·30 |

and then

$$\beta_{mn}^2 = \epsilon_{r_2} k_0^2 - \frac{m^2 \pi^2}{a^2} - \frac{n^2 \pi^2}{b^2} \tag{139}$$

(from eqn. (53)).

The above results are true for $LSM_{mn}$ modes also.

### 17.3. *Improper modes*

In the case of partly sinusoidal and partly hyperbolic $LSE_{mn}$ modes the transverse propagation constant $k_{y_1}$ (in region 1) is imaginary. Putting $k_{y_1} = jk_{y_{1r}}$, where $k_{y_{1r}}$ is a real quantity, eqn. (54) becomes

$$k_{y1r}^2 = \beta_{mn}^2 + \frac{m^2 \pi^2}{a^2} - \epsilon_{req} k_0^2. \tag{140}$$

For the propagation of partly sinusoidal and partly hyperbolic mode, the following condition must be satisfied by eqn. (140)

$$k_{y1r}^2 = \beta_{mn}^2 + \frac{m^2 \pi^2}{a^2} - \epsilon_{req} k_0^2 \geq 0. \tag{141}$$

At cut-off, $\beta_{mn} = 0$, and hence the cut-off frequencies of the partly sinusoidal and partly hyperbolic mode satisfy the following inequality :

$$\frac{m^2 \pi^2}{a^2} - \epsilon_{req} k_0^2 \geq 0$$

or

$$\frac{\omega_c}{2\pi} = f_c \leq \frac{m\pi c}{a\sqrt{\epsilon_{req}}} \tag{142}$$

where $c = 1/\sqrt{\mu_0 \epsilon_0}$

from $m = 0$, at cut-off, we obtain

$$k_{y1r}^2 \text{ (cut-off)} = -\omega_c^2 \mu_0 \mu_r \epsilon_0 \epsilon_{req}. \tag{143}$$

From eqn. (143) it is evident that $k_{y_{11}}$ (cut-off) cannot become positive. Therefore partly sinusoidal and partly hyperbolic $LSE_{0n}$ modes cannot propagate in the dielectric-lined metal rectangular waveguide, and hence are improper modes.

## 17.4. *Propagation characteristics of $LSE_{mn}$ and $LSM_{mn}$ modes*

(i) It is observed from Figs. 3.1 to 4.6 that (*a*) the $a\beta_{mn}$ vs. $ak_0$ characteristics of both $LSE_{mn}$ and $LSM_{mn}$ modes vary almost in a similar fashion; (*b*) in both types of modes the cut-off frequency increases with the mode index $m$ and order of appearance $n$ of modes; (*c*) generally $LSM_{mn}$ modes of type 2 and $LSE_{mn}$ modes of type 1 propagate for a larger frequency range for all values of $d$; (*d*) $LSM_{11}$ mode type 2 is the dominant mode (with lowest cut-off frequency); (*e*) in the cases of all modes of various types, at high frequencies, $ak_0$ vs. $a\beta_{mn}$ curves for the dielectric-lined waveguide approach towards the phase constant *vs.* frequency curve of the completely filled waveguide. The energy is then concentrated practically in the dielectric lining and the inhomogeneous waveguide can be used as a dielectric guide. As a result the losses in the dielectric-lined waveguide increase at high frequency.

(ii) At high frequencies the phase velocity and the group velocity approach asymptotically $1/\epsilon_{r_2}$ times the velocity of light (Figs. 5.1 to 6.3), and the product $v_p v_g/C^2$ for both $LSE_{mn}$ and $LSM_{mn}$ modes approach $1/\epsilon_{r_2}$ for all $d$ and $ak_0$ as shown in Table IV.

**Table IV**

**Product of normalized phase and group velocities**

| $\epsilon_{r_2}$ | $1/\epsilon_{r_2}$ | Dielectric lining thickness $d$ in cm | $v_p v_g/c^2$ | |
|---|---|---|---|---|
| | | | $LSM_{11}$ mode type 2 | $LSM_{21}$ mode type 2 |
| 2·56 | 0·390 | 0·15 | 0·389 | 0·390 |
| | | 0·30 | 0·388 | 0·388 |
| | | 0·40 | 0·389 | 0·390 |
| | | 0·50 | 0·390 | 0·390 |
| 9·0 | 0·111 | 0·15 | 0·110 | 0·111 |
| | | 0·30 | 0·109 | 0·110 |
| | | 0·40 | 0·111 | 0·111 |
| | | 0·50 | 0·110 | 0·109 |

(iii) The percentage bandwidth in the dielectric-lined waveguide cannot be more than 66·6% which happens to be the bandwidth between the $TE_{20}$ and $TE_{10}$ modes of the air-filled waveguide.

(iv) In the case of all the modes of $LSE_{mn}$ and $LSM_{mn}$ types, the total attenuation constant $\alpha_T$ vs. $ak_0$ curves tend to infinity near cut-off frequency, and then most of the curves pass through minima and then approach infinity again at very high frequencies (Figs. 18, 19 and 26). This shows that at high frequencies all the energy is concentrated almost in the dielectric lining which introduces high losses. The attenuation constant of higher order modes helps to assess the order of mode purity. It may be said that the higher the attenuation of the higher order modes the greater is the mode purity of the dominant $LSM_{11}$ mode type 2. It is also observed that the total attenuation constant in the case of $LSM_{11}$ and $LSM_{21}$ modes of type 2 is minimum at $ak_0 = 4{\cdot}0$ and $ak_0 = 7{\cdot}82$ respectively at $d = 0{\cdot}15$ cm.

(v) It is interesting to find that the power handling capacity (temp. rise method) is maximum at the points where the attenuation constant is minimum of the various modes (Table V).

(vi) From Figs. 24, 25 and 26 it is evident that the power handling capacity of the dominant $LSM_{11}$ mode type 2 due to method 2 is higher than that of any other mode for all values of $d$ and $\epsilon_{r_2}$, though the maximum power handling capacity of the higher order $LSE_{mn}$ and $LSM_{mn}$ modes is not significantly less than that of the $LSM_{11}$ mode type 2.

(vii) The maximum transmissible power decreases with the increase of frequency, *i.e.*, with the increase of field concentration and dielectric-lining thickness, and this can be explained by the fact that the power losses in the dielectric increase with $d$ and $ak_0$.

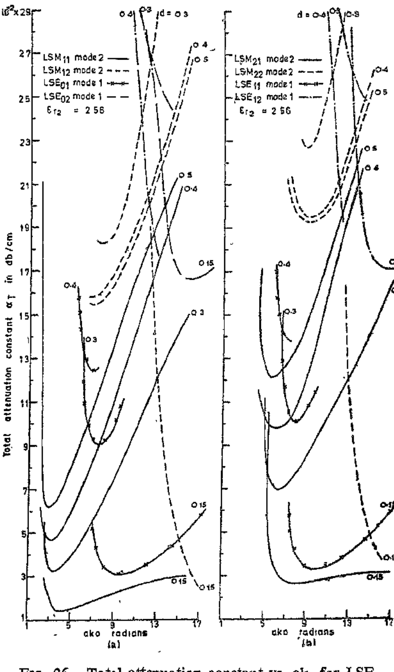


FIG. 26. Total attenuation constant vs. $ak_0$ for $LSE_{mn}$ and $LSM_{mn}$ modes (Parameter being d).

(viii) The phase shift in the dielectric-lined waveguide with respect to the air-filled waveguideis calculated from the relation:

$$\phi_{\text{shift (deg/cm)}} = \frac{2\pi \times 180}{\pi}\left(\frac{1}{\lambda_{g\,(\text{dielectric})}} - \frac{1}{\lambda_{g\,(\text{air})}}\right). \tag{144}$$

Table VI gives the phase shift as a function of frequency for $\epsilon_{r_2} = 2 \cdot 56$ and $d = 0 \cdot 3$ cm.

(ix) The experimental determination of guide wavelength $\lambda_g$ verifies the existence of the $LSM_{11}$ mode type 2. The discrepancy between theoretical and experimental values of $\lambda_g$ and cut-off frequency $f_c$ is very small and it may be ascribed to the approximations involved in the theory.

**Table V**

**Frequency at which power handling capacity is maximum and total attenuation is minimum for $LSM_{mn}$ mode type 2**

| $\epsilon_{r_2}$ | Dielectric lining thickness $d$ in cm | Maximum power handling capacity | | Minimum attenuation | |
|---|---|---|---|---|---|
| | | $ak_0$ in radians | | $ak_0$ in radians | |
| | | $LSM_{11}$ mode type 2 | $LSM_{21}$ mode type 2 | $LSM_{11}$ mode type 2 | $LSM_{21}$ mode type 2 |
| 2·56 | 0·15 | 4·0 | 7·82 | 4·0 | 7·82 |
| | 0·30 | 3·62 | 6·58 | 3·62 | 6·6 |
| | 0·40 | 3·18 | 6·2 | 3·15 | 6·0 |
| | 0·50 | 3·0 | 5·6 | 3·0 | 5·6 |

**Table VI**

**Phase shift-frequency relation $LSM_{11}$ mode 2**

($\epsilon_{r_2} = 2 \cdot 56$; $d = 0 \cdot 3$ cm)

| Frequency in GHz | $g^{(\text{dielectric})}$ $LSM_{11}$ mode 2 | $g^{(\text{airfilled})}$ $TE_{10}$ mode | in deg/cm |
|---|---|---|---|
| 8·355 | 3·3383 | 5·80 | 45·79 |
| 9·399 | 2·8041 | 4·45 | 47·48 |
| 10·444 | 2·4289 | 3·68 | 50·40 |
| 11·488 | 2·1475 | 3·18 | 54·43 |
| 12·533 | 1·9266 | 2·80 | 58·28 |
| 13·577 | 1·7478 | 2·51 | 63·21 |
| 14·620 | 1·5994 | 2·29 | 68·11 |

## 18. Conclusions

The investigations on the dielectric-lined metal rectangular waveguide lead to the following conclusions:

(i) $LSM_{11}$ mode type 2 is the dominant mode.

(ii) $LSE_{01}$, $LSE_{11}$ and $LSE_{21}$ modes of type 1 are improper modes as they do not satisfy the proper boundary conditions at $y = b$ for all $d$ and $\epsilon_{r_2}$.

(iii) Completely hyperbolic modes of either $LSE_{mn}$ or $LSM_{mn}$ types cannot exist in such a structure.

(iv) In general, $LSM_{11}$ mode type 2 has a lower attenuation constant than any other modes.

(v) The maximum bandwidth that can be achieved between the dominant $LSM_{11}$ mode and the next higher order mode $LSM_{11}$ is 66·6 per cent which is the same as that of an airfilled rectangular metal waveguide.

(vi) The power handling capacity due to temperature rise method in the case of the dominant $LSM_{11}$ mode type 2 is generally the highest for all values of $d$ and all frequencies.

(vii) The power handling capacity (temperature rise method) is maximum when the total attenuation is minimum, though this is less than that of the $TE_{10}$ mode in an airfilled waveguide.

(viii) The power handling capacity calculated by the method of temperature rise is lower than that obtained by the breakdown field method.

(ix) The measurement of guide wavelength $\lambda_g$ establishes the existence of the dominant $LSM_{11}$ mode type 2 at X- and Ku-bands.

(x) Measurement of $\lambda_g$ at Ka-band proves the existence of higher order $LSM_{mn}$ modes especially of type 2.

(xi) There is a fair agreement between the theoretical and experimental results of the guide wavelength at all frequencies.

(xii) Experimental values of cut-off frequencies agree well with the theoretical values for $LSM_{11}$ mode type 2 for various values of $d$ and $\epsilon_{r_2}$.

(xiii) The dielectric-lined metal rectangular waveguide may find application as a phase shifter, slow-wave structure and probably as a high frequency transmission line.

Further work is being carried out on the characteristics of such structures with very thin dielectric linings and also on the coupling between modes.

## References


1. Frank, N. J. — *Waveguide Handbook*, M.I.T. Radiation Laboratory Report 9, Cambridge, Mass., U.S.A., 1942.
2. Pincherle, L. — Electromagnetic waves in metal tubes filled longitudinally with two dielectrics, *Phys. Rev.*, 1944, **66**, 118–130.
3. Montgomery, C. G., Dicke, R. H. and Purcell, E. M. — *Principles of microwave circuits*, M.I.T. Radiation Laboratory Series, McGraw-Hill, New York, 1948, **8**, 385–389.
4. Van Bladel, J. — Expandability of a waveguide field in terms of normal modes, *J. Appl. Phys.*, 1951, **22**, 68–69.
5. Van Bladel, J. and Higgins, T. J. — Cut-off frequency in two dielectric layered rectangular waveguide, *J. Appl. Phys.*, 1951, **22**, 329–334.
6. Weeks, W. L. — Propagation constant in rectangular waveguide filled with ferrite, *I.R.E. Trans.*, 1959, *MTT* **9**, 294–295.
7. Bui Van, R. E. and Gagne, R. R. J. — Propagation of waves in rectangular waveguides containing dielectric layers in the H-plane, *I.N.T.J. Electronics*, 1972, **32**, 353–360.
8. Bui Van, R. E. and Gagne, R. R. J. — Dielectric losses in an H-plane loaded rectangular waveguides, *I.E.E.E. Trans.*, 1972, *MTT* **20**, 621–623.
9. Marcuvitz, N. — *Waveguide Handbook*, McGraw-Hill Book Co., New York, 1951, pp. 387–393.
10. Chambers, L. I. G. — Compilation of the propagation constants of an inhomogeneously filled waveguide, *Brit. Journ. Appl. Phys.*, 1952, **3**, 19–21.
11. Malinovsky, K. V. and Angelakos, D. J. — *Propagation in inhomogeneously filled guides*, University of California, Berkeley, Calif., USA, Institute of Engineering Research, 1959, Series No. 60, Issue No. 125.
12. Berk, A. D. — Variational principles of electromagnetic resonator and waveguides, *I.R.E. Trans.*, 1956, *AP*-**4**, 104–111.
13. Collin, R. E. and Valliancourt, R. M. — Application of Rayleigh-Ritz method to dielectric steps in waveguides, *I.R.E. Trans.*, 1957, *MTT*-**5**, 177–189.
14. Collin, R. E. — *Field theory of guides*, McGraw–Hill Book Co., Inc., New York, 1960, pp. 22–27; 104–118; 127–128 and 170–181.
15. Vartiniau, P. H. Ayres, W. P. and Helgesson, A. L. — Propagation in dielectric slab loaded rectangular waveguide, *I.R.E. Trans.*, 1958, *MTT*-**6**, 215–222.
16. Bland, G. F. and Franco, A. G. — Phase shift characteristics of dielectric-loaded waveguide, *I.R.E. Trans.*, 1962, *MTT*-**10**, 492–496.
17. Seckelmann, R. — Propagation of TE modes in dielectric-loaded waveguides, *I.E.E.E. Trans.*, 1966, *MTT*-**14**, 518–527.

18. CHATTERJEE, S. K. AND CHATTERJEE, R. Dielectric-loaded waveguides; review of theoretical solutions, *Journ. Inst. Electronic and Radio Engineers*, 1965, **30**, Pp. 145–160; 195–205; 259–588 and 353–364.

19. HOWARD, R. WITT, RITA E. BISS AND PRICE, E. L. Propagation characteristics of waveguides containing parallel sheets of finite conductivity, *I.E.E.E. Trans.*, 1967, *MTT*-**15**, 232–234.

20. EBERHARDT, N. Propagation in the off-centre E-plane dielectrically-loaded waveguides, *I.E.E.E. Trans.*, 1967, *MTT*-**15** (5), 282–289.

21. GARDIOL, F. E. Higher order modes in dielectrically-loaded waveguides, *I.E.E.E. Trans.*, 1968, *MTT*-**16** (11), 919–924.

22. FINDAKLY, T. K. AND HASKAL, H. M. On the design of the dielectric-loaded waveguides, *I.E.E.E. Trans.*, 1976, *MTT*-**24** (1), 39–43.

23. TSANDOULAS, G. N. Propagation in dielectric-lined square waveguides, *I.E.E.E. Trans.*, 1975, *MTT*-**23**, 406–410.

24. BARCELI, T. C. Design of cylindrical surface waveguides with dielectric and magnetic coating, *Proc. I.E.E.*, 1961, **108**, pt. C, 386.

25. JACOB, M. AND HAWKINS, G. H. *Elements of Heat Transfer*, John Wiley and Sons Inc., New York, 1957, p. 157.

# Seminar on 'Management of R & D in Industry'

The Hyderabad-based Indian Research and Seminar Centre is organising an eight-day seminar on ' Management of R & D in industry ' at Hotel Ashoka, Bangalore. Slated to start on January 1, 1980, this course will cover the philosophy, planning and functioning of R & D, selection of R & D personnel, finance and evaluation, tools and processes, new industrial products and technological problems and is likely to be useful to all involved in R & D.

The faculty, according to the Centre's press release, are drawn from established and reputed institutions. The convener of the seminar is Dr. Anand Khare.

The registration fee per participant is Rs. 5,000, which covers board and lodging at Hotel Ashoka for eight days and lecture material. The last date for registration is November 30, 1979.

Participants desirous of contributing original papers to the seminar should send immediately a 300-word synopsis to the Centre.

Further particulars can be had from the Indian Seminar and Research Centre, 8–2–248/B/1, Journalist Colony, Road No. 3, Banjara Hills, Hyderabad 500 034.